Obscured asymptotic giant branch stars in the Magellanic Clouds - II. Near-infrared and mid-infrared counterparts

Zijlstra, A.A.; Loup, C.; Waters, L.B.F.M.; Whitelock, P.A.; Guglielmo, F.

DOI
10.1093/mnras/279.1.32

Publication date
1996

Published in
Monthly Notices of the Royal Astronomical Society

Mon. Not. R. Astron. Soc. **279,** 32–62 (1996)

Obscured asymptotic giant branch stars in the Magellanic Clouds – II. Near-infrared and mid-infrared counterparts

Albert A. Zijlstra,[1] Cecile Loup,[2,3] L. B. F. M. Waters,[2,4] P. A. Whitelock,[5] Jacco Th. van Loon[1] and F. Guglielmo[6]

[1]*European Southern Observatory, Karl-Schwarzschild-strasse 2, D-85748 Garching bei München, Germany*
[2]*Space Research Groningen, PO Box 800, NL 9700-AV Groningen, the Netherlands*
[3]*Institut d'Astrophysique de Paris, 98-bis Boulevard Arago, F-75014 Paris, France*
[4]*Astronomical Institute 'Anton Pannekoek', University of Amsterdam, Kruislaan 403, NL-1098 SJ Amsterdam, the Netherlands*
[5]*South African Astronomical Observatory, PO Box 9, Observatory 7935, South Africa*
[6]*Sterrewacht Leiden, PO Box 9513, NL-2300 RA Leiden, the Netherlands*

Accepted 1995 September 8. Received 1995 September 6; in original form 1994 December 29

ABSTRACT

We have carried out an infrared search for obscured asymptotic giant branch (AGB) stars in the Magellanic Clouds. Fields were observed in the vicinity of *IRAS* sources with colours and flux densities consistent with such a classification. The survey uncovered a number of obscured AGB stars as well as some supergiants with infrared excess. We present photometry of the sources and discuss the colour diagrams and bolometric luminosities. One of the supergiants is close to the maximum luminosity allowed for red supergiants, implying a progenitor mass around 50 $M_\odot$. Its late spectral type (M7.5) is surprising for such a massive star. Most of the AGB stars are luminous, often close to the classical limit of $M_{bol} = -7.1$. To determine whether the stars are oxygen-rich or carbon-rich, we have acquired narrow-band mid-infrared photometry with the ESO TIMMI camera for several sources. All but one are found to show the silicate feature and therefore to have oxygen-rich dust; the colours of the remaining source are consistent with either an oxygen-rich or a carbon-rich nature. A method to distinguish carbon and oxygen stars based on $H-K$ versus $K-[12]$ colours is presented. We discuss several methods of calculating the mass-loss rate: for the AGB stars the mass-loss rates vary between approximately 5×10^{-4} and 5×10^{-6} $M_\odot$ yr^{-1}, depending on the assumed dust-to-gas mass ratio. We present a new way to calculate mass-loss rates from the OH maser emission. We find no evidence for a correlation of the mass-loss rates with luminosity in these obscured stars. Nor do the mass-loss rates for the Large Magellanic Cloud (LMC) and Small Magellanic Cloud (SMC) stars differ in any clear systematic way from each other. Expansion velocities appear to be slightly lower in the LMC than in the Galaxy. Period determinations are discussed for two sources: the periods are comparable to those of the longer-period Galactic OH/IR stars. All of the luminous stars for which periods are available have significantly higher luminosities than predicted from the period–luminosity relations.

Key words: stars: AGB and post-AGB – circumstellar matter – stars: mass-loss – Magellanic Clouds – infrared: stars.

1 INTRODUCTION

One of the least understood stages of stellar evolution occurs on the upper part of the asymptotic giant branch (AGB). After the onset of thermal pulses, when the star alternates between helium- and hydrogen-shell burning, mass loss from the star starts to increase. Mass-loss rates as high as 10^{-4} $M_\odot$ yr^{-1} have been found for Galactic AGB stars, causing the removal of almost the entire hydrogen envelope. Since the nuclear-burning rate on the AGB is less than 10^{-6} $M_\odot$ yr^{-1}, it is clear that mass loss dominates the evolution. After the high-mass-loss phase ends, the star

rapidly increases in temperature and evolves towards the planetary nebula phase. All stars with initial masses less than ~ 6–$8\ M_\odot$ (depending on metallicity) are expected to pass through this phase.

Knowledge of the AGB evolution is hampered by two major problems. First, no adequate theoretical formulation of mass loss exists, partly because the driving mechanism is not fully understood (for a review see Hearn 1989). Secondly, no accurate distances are known for the majority of evolved AGB stars. In the Milky Way, only the bulge provides a large sample of mass-losing AGB stars at fairly uniform distances. The stars in the outer bulge have been the subject of extensive studies (e.g. Whitelock, Feast & Catchpole 1991), but this sample contains only old, low-mass stars and the distance spread is still quite large. The central part of the bulge may contain a sample of more massive stars at a known distance, but the large extinction makes these difficult to study. In contrast, the LMC provides a sample of AGB stars at a well-determined distance, which includes both low-mass and high-mass stars. It is for this reason that the study of AGB stars in the Magellanic Clouds is important.

Until recently, Magellanic Cloud studies were limited to optically visible AGB stars. This is a severe limitation, since it is well known that many Galactic AGB stars experience sufficiently high mass-loss rates to be optically obscured. The known LMC stars were therefore biased towards stars with low mass-loss rates, which have much less optical obscuration. Reid, Tinney & Mould (1990) compiled a catalogue of *IRAS* sources aimed at finding mass-losing AGB stars. Using this catalogue, Reid (1991) found evidence for the existence of obscured AGB stars in the LMC. He discovered a number of near-infrared sources very close to the *IRAS* position, in most cases without optical counterparts. In contrast, many of the suggested optical identifications of Reid et al. (1990) were at considerable distance from the *IRAS* source. Wood et al. (1992) also found a number of near-infrared point sources without optical counterparts in the vicinity of *IRAS* sources, comprising both AGB stars and mass-losing supergiants. They showed from OH observations and period determinations that their sources were closely related to the Galactic OH/IR stars. The LMC is close to the detection limit of *IRAS* for AGB stars, and it is likely that in these studies only the most luminous objects were found. This is especially clear in the sample of Wood et al., who observed the brightest *IRAS* sources and found very luminous counterparts: whereas Reid (1991) found $M_{\rm bol} = -5$ to -6, Wood et al. found for all their sources $M_{\rm bol} < -6$.

We have used the catalogue of stellar *IRAS* sources in the Magellanic Clouds (Loup, Zijlstra & Waters 1995, Paper I) to identify possible obscured AGB stars. The selection was performed both on expected $[12]-[25]$ *IRAS* colours and on flux density. Near-infrared imaging and photometry were obtained to identify which sources were obscured AGB stars. As was already found by Reid et al. (1990), the main confusion in the sample is caused by supergiants which, however, are easy to identify. In the following sections we present the source selection and observations, and discuss the photometry of the objects. In Section 7 we discuss the results of 10-μm imaging in narrow bands for five sources, from which we derive information on whether the stars are oxygen-rich or carbon-rich. Mass-loss-rate determinations are discussed in Section 9. Finally, for two objects with previous photometry, we discuss period determinations. Our results significantly enlarge the known sample of obscured AGB stars.

2 SOURCE SELECTION

There are two *IRAS*-based catalogues available for the Magellanic Clouds which go significantly deeper than the Point Source Catalog (PSC). The large catalogue of Schwering & Israel (1990) (see also Schwering & Israel 1989 and Schwering 1989) was derived from the pointed observations. Reid et al. (1990) used co-adding scans to increase the sensitivity and produced a catalogue for part of the LMC. Both used the Deep Sky Mapping data which are not used in e.g. the Faint Source Catalog (FSC), and as a result go deeper in the more crowded regions. [However, the FSC also covers the halo of the LMC and SMC which was not included in the Deep Sky Mapping programme. Zijlstra et al. (1994) find, for the planetary nebulae in the LMC detected by *IRAS*, that there is good agreement between the FSC and the Schwering & Israel catalogue, for those objects in common.]

Loup et al. (1995, Paper I) have combined these catalogues to identify evolved stars with infrared excess in the LMC. They show that only AGB stars in the LMC with high mass-loss rates ($> 5 \times 10^{-6}\ M_\odot\ {\rm yr}^{-1}$) and luminosity ($L > 10^4\ L_\odot$) are within the detection limits of *IRAS*. Their selection of the most likely stellar sources in the *IRAS* data base is based on *IRAS* colours, using the source-separation diagram of Pottasch et al. (1988), as well as on the expected flux levels. After applying their selection criteria and removing 131 foreground stars, they are left with more than 100 'best candidate' sources. From this list, we selected about 65 sources for infrared imaging and photometry. There is significant overlap with the sample of Reid (1991): of the 13 sources in his sample, 12 were independently also selected by us. Furthermore, there is one source in common with Wood et al. (1992). Some of the selected *IRAS* sources were identified with a bright star on the ESO-*R* Schmidt plates, making imaging observations unnecessary. In a number of cases we also found optical counterparts from a literature survey using SIMBAD. Because the source selection was performed using a preliminary version of the catalogue of Paper I, there were still a few likely foreground stars in the sample.

At these low flux levels, the uncertaintities on the *IRAS* fluxes can be the limiting factor on our ability to select AGB-star candidates. The uncertainties are discussed in more detail in Paper I. The *IRAS* detection limit depends on the crowding: Schwering & Israel quote general sensitivity limits of 0.15 and 0.22 Jy at 12 and 25 μm, respectively, but find a few sources with fluxes as low as 0.07 Jy. They note that the noise is mostly due to the LMC background and that the detectors themselves have lower noise. In addition, there are differences between the absolute calibrations of Schwering & Israel and Reid et al., with the latter being 25 per cent lower at 25 μm. From a comparison between sources in common between these two catalogues and the PSC, Loup et al. (Paper I) derive a typical uncertainty on $C_{21} = \log[12S_{25}/(25S_{12})]$ of 0.25, corresponding to 1.4 mag,

largely systematic and mostly arising from the 25-μm flux. At 12 μm, the statistical error varies from 1 mag for the faintest source to 0.2 mag for the remainder. The 60- and 100-μm fluxes are affected by confusion in some regions with high background flux, leading to flux ratios normally associated with H II regions: this may have eliminated some true AGB stars. The high success rate of the present survey indicates that the uncertainties are not disastrous, but complete samples cannot be obtained from the *IRAS* catalogues. It is not possible to derive uncertainties for individual sources.

Table 1 lists the selected sources, and where they were observed. Also listed is whether a counterpart was found on the ESO *R*-plates, labelled 'bright' if $m_R \lesssim 10$. The star symbols indicate objects discovered by Reid (1991) and Wood et al. (1992). For each object we list the original name of the infrared source from Schwering & Israel (1990) or Reid et al. (1990) in the first or second column. The third column gives the *IRAS*-PSC name, or if the object is not in the PSC we give the 1950 coordinates in the form normally used for *IRAS*-PSC sources but without the prefix. In the cases where we could identify a likely optical counterpart in the literature, its name is listed if it was known before *IRAS*, and also the spectral type if known. The naming convention is as follows: *IRAS* source names are PSC (*IRAS* Point Source Catalog), TRM (Reid et al. 1990), LI-LMC and LI-SMC (Schwering & Israel 1990). Names of optical sources are HV (Harvard Variable star: Payne-Gaposchkin & Gaposchkin 1966), WOH (Westerlund, Olander & Hedin 1981: 'SG' for suspected supergiant, 'G' for suspected giant), RMMP (Rebeirot et al. 1983), SP (Sandulaek & Philip 1977) and SK (the objective-prism survey of Sandulaek 1970). The names used in the remainder of the paper are indicated in boldface.

3 OBSERVATIONS

3.1 Near-infrared imaging

Near-infrared imaging of the selected sources was carried out on the MPI 2.2-m telescope at La Silla on 1993 January 2–6. We used IRAC-2, which is a 256 × 256 NICMOS-3 infrared array, with standard ESO *J*, *H* and *K* filters. The weather was generally not photometric. During two nights cirrus appeared to be present, and the other two suffered from very high humidity. Some hours were lost because of humidity. The seeing was mostly 1 arcsec or better in the near-infrared. On the first three nights we used a pixel scale of 0.27 arcsec pixel^{-1}, which gives a field of view of 69 arcsec. However, this field may be insufficient for some sources as the uncertainty in the *IRAS* position can be large for faint sources in confused regions. On the fourth night we used a larger scale of 0.49 arcsec pixel^{-1}, re-observing a number of fields where the smaller field either did not show an obvious counterpart or did not contain sufficient stars for astrometric purposes. A problem with the large scale is that the stellar images are undersampled, making it more difficult to extract reliable photometry.

Each field was observed for 1 min per filter, followed by a 1-min exposure on-sky. For bright objects (including standard stars) the telescope was defocused to prevent the array becoming non-linear. Dome flats were taken for flat-fielding. In total about 50 fields were imaged. Most fields were found to contain an obvious, red object, in a few cases visible only at *K*. In other cases the infrared source was visible at *J*, *H* and *K*, but not on the finding chart which was made from the ESO-*R* Schmidt plates. Other objects were also bright on the *R* plates. There were a few fields without a likely candidate. In some cases the red star was more than 30 arcsec away from the *IRAS* position and the association was not certain. Fig. 1 shows as an example the IRAC-2 images at *J* and *K* of 05329 − 6709 (TRM60), one of the reddest objects in our sample.

3.2 Near-infrared photometry

Near-infrared (*JHKL*) photometry was carried out on 1993 February 2–8, using the Mk III photometer on the SAAO 1.9-m telescope at Sutherland. A few additional observations were obtained during a run in 1993 March. All sources detected with IRAC-2 were observed. In addition, sources with bright *R* counterparts were observed, for which imaging was unnecessary, and a few *IRAS* sources for which counterparts had not yet been found. In the last case we attempted to find the counterpart by scanning the field using the *K* filter. The SAAO photometer uses a dewar with an InSb detector and apertures of 3, 6, 9, 12 or 18 arcsec. If available, we used the IRAC-2 images to ensure that no other star was included in the aperture, or else to correct the derived magnitudes for the contaminating star. The photometry was calibrated using the standards HR 0077 for the SMC and HR 2015 for the LMC. All observations were transformed to the system defined by Carter (1990). The standard SAAO extinction law was assumed.

Observing conditions were generally good. One night was lost because of clouds, and during several other nights ridge cloud appeared towards the end of the night. Seeing was commonly 1–2 arcsec at the beginning of the night, significantly worsening at the end, especially before the appearance of ridge clouds. The aperture used was adjusted according to the seeing. All six usable nights were photometric.

3.3 Mid-infrared imaging and photometry

We used the ESO 10-μm camera TIMMI (Käufl et al. 1992) to observe six objects from our source list. The observations were carried out at the 3.6-m telescope at La Silla on 1993 December 1–3. The conditions were photometric. TIMMI contains a 64 × 64-element gallium-doped silicon array with good cosmetic quality (one dead pixel) and a quantum efficiency of about 25 per cent. We used the *N*-band filter ($\lambda_c = 10.10$ μm, $\delta\lambda = 5.10$ μm) as well as two narrow-band filters centred on the silicate and silicate–carbide features ($\lambda = 9.70$ μm, $\delta\lambda = 0.49$ μm; $\lambda_c = 11.30$ μm, $\delta\lambda = 0.57$ μm, respectively). The 40-mm lens, yielding a scale of 0.45 arcsec per pixel and a field of view of 29 × 29 arcsec^2, was used.

The normal observing procedure is to chop and nod so that two reference fields on both sides of the source field are continuously subtracted from the source field. The chopping frequency is several hertz and nodding is done once or twice per minute. We selected a chop of 8 arcsec, so that both reference frames would also contain the (point) source. This gives a significant improvement in signal-to-

Table 1. Selected sources and observing log.

LI-SMC/LMC	TRM	PSC (B1950)	IRAC-2 [a]	SAAO[a]	R-plate[b]	TIMMI[a]	optical	type	comment
LI-SMC 225		PSC00165−7418	y	y	b		**VV Tuc**	M4	1
LI-SMC 005		PSC00350−7436	y	y	f			Ce+	
LI-SMC 185		PSC01074−7140	y	y	b	y	**HV12956**	M5e	2
LI-LMC1825		PSC04286−6937	y	y	n				
LI-LMC1844		PSC04374−6831	y	y	n				
LI-LMC0004		PSC04407−7000	y	y	n	y			
LI-LMC0057		PSC04496−6958	y	y	f				3
LI-LMC0060		PSC04498−6842	y	y	f	y			4
LI-LMC0099		PSC04518−6852	n						
LI-LMC0141		PSC04539−6821	y	y	n				
LI-LMC0198		PSC04557−6753	y	y	f				5
LI-LMC0183		PSC04553−6933		y	b		**WOH SG071**	M2	
LI-LMC0203		PSC04559−6931	y	y	b		**HV12501**	M1.5	6
LI-LMC0253		PSC04581−7013	y	y	b		**HV2255**	M4	
LI-LMC0273		PSC04588−6811	n						
LI-LMC0297		PSC05003−6712		y	f				
LI-LMC0310		PSC05009−6616		y	f				
LI-LMC0463	TRM009	PSC05073−6752	n						
	TRM133	05079−6542	n						
LI-LMC0528	TRM023	PSC05099−6740	y	y	f				
LI-LMC0567	TRM100	PSC05110−6616	n						
⋆LI-LMC0570	TRM004	PSC05112−6755	y	y	n	y			
⋆LI-LMC0571	TRM024	PSC05112−6739	y	y	n				
⋆**LI-LMC0578**	TRM072	05117−6654		y	n				
LI-LMC1880		PSC05128−6455	y	y	n				
LI-LMC0671		PSC05150−6942	n						
LI-LMC0732		PSC05171−7048	y	y	b		**HV928**	M3	7
⋆LI-LMC0793	TRM020	PSC05190−6748		y	n				
⋆	**TRM088**	05203−6638		y	n				
LI-LMC1883		PSC05208−6459		y	f		**WOH G281**	M	
	TRM105	05215−6547		y	b		**HD271191**	B0Iab	8
LI-LMC0932	TRM108	PSC05235−6544		y	b		**HV12793**	M3/4	9
LI-LMC0957	TRM016	PSC05242−6748	n						
	TRM096	05270−6624		n					
	TRM073	05276−6656		y	b		**HV963**	M2/3I	
LI-LMC1092		PSC05278−6942	n						
LI-LMC1103		PSC05281−6915	y	y	b		**SP47-14**	M1	
	TRM045	05283−6723		n					
LI-LMC1116	TRM114	05288−6731		n					
LI-LMC1130	TRM099	PSC05289−6617	y	y	b				
LI-LMC1137		PSC05291−6700	y	y	f				
LI-LMC1157		PSC05295−7121	y	y	n	y			
	TRM103	05298−6552	n						
LI-LMC1170	TRM049	PSC05299−6720		y	b		**SP45-34**	M1Ia	
LI-LMC1172		PSC05300−6859	y	y	b		**SP46-44**	M1Ia	
⋆LI-LMC1177	TRM079	PSC05300−6651	y	y	f				
LI-LMC1190	TRM046	PSC05304−6722		y	b				
LI-LMC1223		PSC05313−6920		y	b		**HV12998**	M1	10
LI-LMC1234	TRM089	PSC05315−6631	y	y	b		**HV990**	M2I	
⋆LI-LMC1238	TRM101	PSC05316−6604	y	y	b		**WOH SG374**	M6	11
LI-LMC1241	TRM087	05318−6642		y	b		**SP52-1**	M3/4I	
⋆**LI-LMC1259**	TRM112	05321−6744		y	b				
⋆LI-LMC1286	TRM060	PSC05329−6709	y	y	n	y			
LI-LMC1304	TRM063	PSC05334−6706	y	y	b		**HV5933**	M4I	
LI-LMC1341		PSC05346−6949	n						
LI-LMC1345		PSC05348−7024	y	y	n				
LI-LMC1360	TRM062	05354−6704		y	b		**HV2700**	M1/2Iab	
LI-LMC1366	TRM068	PSC05355−6657		y	b				
⋆LI-LMC1382	TRM077	PSC05360−6648	y	y	n				
LI-LMC1602	TRM135	PSC05433−6728	y	y	b				
LI-LMC1765		PSC05506−7053	y	y	n				
LI-LMC1768		PSC05522−7120	n						
LI-LMC1780		PSC05540−6533	n						
LI-LMC1790		PSC05558−7000	y	y	n				
LI-LMC1795		PSC05568−6753	y	y	b				
LI-LMC1803		PSC05588−6944	n						

[a] y: detected, n: not detected, blank: not observed; [b] b: bright, f: faint, n: not detected.

1. Also known as HV6325. 2. Invisible on finding chart (R), but bright on TV screen. 3. AGB star is western component of double star. 4. Counterpart is eastern half of very faint double, just visible on *R* plate. 5. Just visible on *R* plate. 6. Also known as RMMP61. Spectral type from Wood et al. (1983). 7. Also known as ZZ Men, WOH SG215, RMMP269. 8. Also known as SK – 65 52. 9. Also known as WOH SG257. 10. The HV star is also known as WOH SG369, RMMP519 and SP 47-22. There is a second star visible on the *R* plate much nearer the *IRAS* position, for which no photometry is available. 11. The star is south of the *IRAS* source, which was outside the IRAC field. It is possible that there is an obscured star nearer the *IRAS* position.

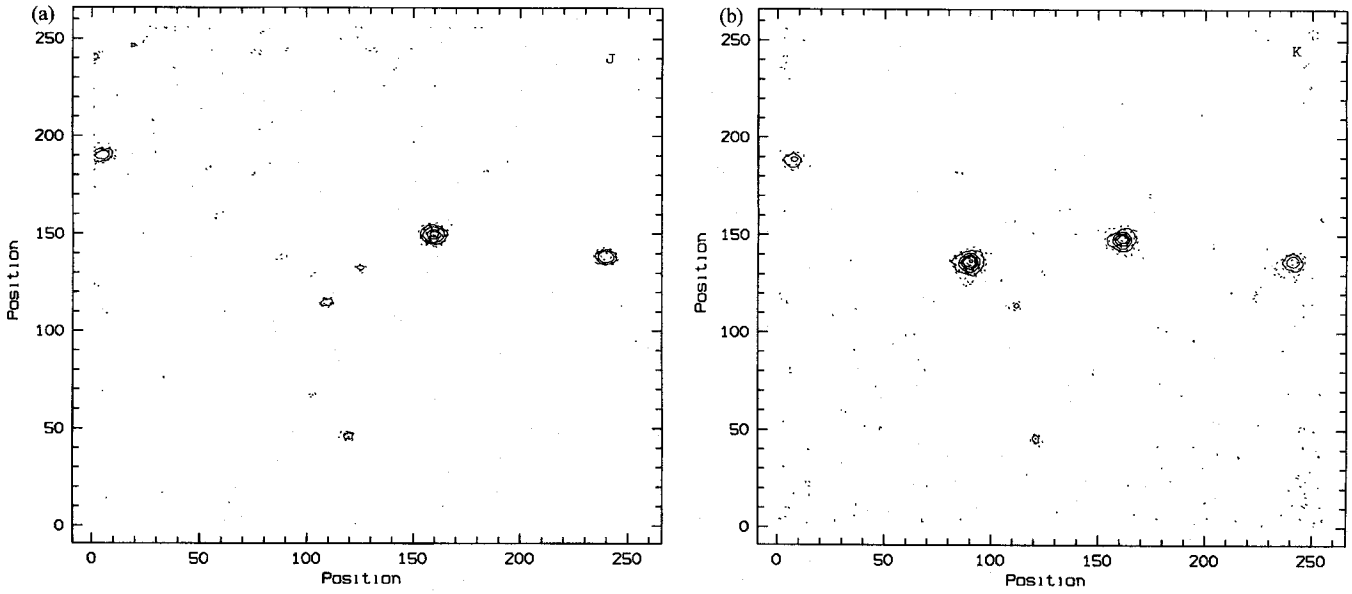

Figure 1. Contour plots of the area around 05329 – 6709 at *J* and *K*.

noise ratio for point sources. In some cases one of the two reference frames could not be used because the source fell too close to the edge of the field. The telescope is essentially diffraction-limited at 10 μm (the first Airy ring has a diameter of 1.4 arcsec) and we did not expect to resolve any of our sources. Integration times of approximately 45 min per source per filter were used. Flat-fielding was done by measuring a standard star at approximately 10 positions on the array, and fitting a two-dimensional parabola to the measured values. The correction can reach a factor of 2 near the edges of the array but is less than 20 per cent over most of the array. This was the reason why measurements close to the edge of the array were not used. The procedure does not correct for pixel-to-pixel variations and leaves a residual uncertainty which we estimate to be about 5 per cent.

The final frames contain one 'positive' and two 'negative' sources, 17 pixel apart. The positive stellar image contains twice as much stellar light as each of the two negative stellar images. To derive reliable magnitudes, as well as reliable estimates of their accuracies, we derived 'magnitude profiles' by summing over a circular area and subtracting the locally determined background, taking circles with a diameter increasing from 3 to 30 pixel. This was performed for both the programme star and the calibrator, and the two profiles were then subtracted. Ideally, this would yield a flat curve – i.e. the diameter of the circle should not affect the differential magnitude, as long as it is the same for the programme and the calibration star. Partly because of seeing variations, in practice for each source we found a range of diameters within which the differential magnitude profile (hereafter DMP) was flat within the noise, with deviations occurring both close to the centre of the stellar image and at large distances. The differential magnitude was derived by averaging the magnitude estimates in the flat part of the DMP. The advantage is that more accurate magnitudes are obtained and a reliable estimate of the accuracy is derived simultaneously: we used the standard deviation of the points with respect to the mean. We used MIDAS to process the images.

This technique was applied only to the 'positive' stellar images: the negative images were normally too close to the edge of the array to allow the calculations with larger circles. We therefore used the 'negative' stellar images as a cross-check only. Digital filtering is normally used in the standard TIMMI reduction software to remove high-frequency variations of the background: this gives an improvement in image quality owing to the fact that the point-spread function is well sampled. However, it left the photometry as well as its accuracy essentially unaffected and we therefore did not apply the digital filtering.

As calibrator we used γ Ret, for which we adopt magnitudes of -0.71 at N, -0.73 at 9.7 μm and -0.77 at 11.3 μm. [These values come from the (unpublished) ESO system; Bouchet et al. (1989) derive magnitudes which are about 0.05 mag fainter.] The N band showed significant atmospheric extinction terms of 0.32 and 0.13 mag per airmass for the first and second nights, respectively. For the 9.7-μm band, which coincides with strong atmospheric O_3 absorption, values of 1.4 and 0.6 mag per airmass were determined on the first and second nights, respectively, and the 11.3-μm band showed an extinction of 0.26 mag per airmass for both nights. The estimated accuracy of the extinction is ~ 20 per cent; this is included in the uncertainties of the derived magnitudes. Our faintest source was detected at an N-band magnitude of about 7.2 ± 0.1 in 45 min, in good agreement with the expected sensitivity of $m_N = 6.3$ at 10σ in 1 h (Käufl et al. 1992).

4 RESULTS

Table 2 lists positions for those objects for which a near-infrared counterpart was found close to the *IRAS* source, either on the IRAC-2 image or via scanning of the field. If an optical counterpart was identified, its position was mea-

sured on the ESO *R* plate, or taken from the Guide Star Catalogue for stars included therein. For stars not detected on the *R* plates, the position was determined from the IRAC-2 image relative to field stars. The sources found through field scanning have positions accurate to ~10 arcsec. For the other sources the 1σ accuracy is about 0.5 arcsec. Table 2 lists the positional difference between the near-infrared and the *IRAS* sources. In three cases the difference is so large that the association is doubtful.

For those sources in common with Reid (1991), the differences between our and Reid's positions are listed in Table 2. The positions are generally in good agreement. Differences around 10 arcsec are found for 04496 – 6958 and 05112 – 6739. There is poor agreement for one source only: LI-LMC1259 (TRM112), where the difference is 41 arcsecc (mostly in right ascension). (In addition, LI-LMC0578 has a difference of 15 arcsec, but for this source our position is not very accurate.) Reid suggests that the source may be extragalactic in nature, but the difference in position makes it likely that an error was made in the identification of the optical counterpart. The object is located in a star-forming region and coincides with a bright knot on the

Table 2. Measured positions.

name	NIR source RA DEC (J2000)	IRAS source RA DEC (J2000)	Δ (″)	Reid (1991) RA DEC (J2000)	Δ (″)	comments
VV Tuc	00 18 53.7 −74 01 57	00 18 50.5 −74 02 15	23			
00350−7436	00 36 59.8 −74 19 50	00 37 00.3 −74 19 47	4			
HV12956	01 09 2.32 −71 24 09	01 09 03.0 −71 24 08	4			
04286−6937	04 28 30.3 −69 30 49	04 28 30.6 −69 30 46	4			
04374−6831	04 37 22.8 −68 25 03	04 37 22.2 −68 25 17	14			
04407−7000	04 40 28.4 −69 55 12	04 40 28.0 −69 55 14	2			
04496−6958	04 49 18.6 −69 53 13	04 49 17.8 −69 53 13	4			
04498−6842	04 49 41.4 −68 37 50	04 49 40.8 −68 37 50	3			
04539−6821	04 53 46.3 −68 16 12	04 53 46.8 −68 16 26	14			
04557−6753	04 55 38.9 −67 49 10	04 55 38.1 −67 48 47	23			
WOH SG071	04 55 03.2 −69 29 13	04 55 02.4 −69 29 13	4			
HV2255	04 57 43.3 −70 08 50	04 57 43.7 −70 08 59	9			
05003−6712	05 00 19.1 −67 07 57	05 00 19 −67 08 03	6			
05009−6616	05 01 03.8 −66 12 40	05 01 04.1 −66 12 43	3			
05099−6740	05 10 02.8 −67 35 48	05 09 54.7 −67 36 42	47			
05112−6755	05 11 10.6 −67 52 11	05 11 10.2 −67 52 17	7	05 11 09.0 −67 52 07	10	
05112−6739	05 11 13.8 −67 36 30	05 11 13.4 −67 36 25	5	05 11 14.3 −67 36 22	9	
LI-LMC0578	05 11 37 −66 51 00	05 11 41.2 −66 51 12	28	05 11 38.6 −66 51 12	15	a,b
05128−6455	05 13 04.6 −64 51 40	05 13 04.2 −64 51 39	19			
HV928	05 16 38.4 −70 45 41	05 16 37.2 −70 45 35	8			
05190−6748	05 18 57 −67 45 00	05 18 56.2 −67 45 25	25	05 18 56.1 −67 44 55	7	
TRM088	05 20 20 −66 35 45	05 20 21.0 −66 36 00	16	05 20 18.7 −66 35 47	8	a,b
WOH G281	05 21 03.6 −64 56 43	05 21 03.3 −64 56 40	3			a
HD271191	05 21 43.0 −65 44 57	05 21 42.2 −65 45 07	11			b
HV12793	05 23 43.6 −65 42 00	05 23 43.1 −65 41 57	5			
HV963	05 27 34.5 −66 53 31	05 27 36.5 −66 53 43	17			
SP47-14	05 27 47.6 −69 13 21	05 27 46.6 −69 13 25	7			b
05289−6617	05 29 02.1 −66 15 27	05 29 02.0 −66 15 26	1			
05291−6700	05 29 07.6 −66 58 15	05 29 06.0 −66 57 48	28			
05295−7121	05 28 40.8 −71 19 13	05 28 49.2 −71 19 26	43			
SP45-34	05 29 55.1 −67 18 37	05 29 55.0 −67 18 33	4			
SP46-44	05 29 42.3 −68 57 18	05 29 42.8 −68 57 20	4			
05300−6651	05 30 04.0 −66 49 24	05 30 04.5 −66 49 04	20	05 30 03.5 −66 49 25	4	
05304−6722	05 30 21.0 −67 20 05	05 30 20.7 −67 20 14	9			
HV12998	05 31 04.2 −69 19 04	05 31 01.5 −69 18 45	24			
HV990	05 31 37.0 −66 30 08	05 31 36.5 −66 29 48	20			
WOH SG374	05 31 47.5 −66 03 40	05 31 45.9 −66 03 51	15	05 31 47.4 −66 03 40	1	
SP52-1	05 31 53.5 −66 40 43	05 31 55.4 −66 40 25	21			
LI-LMC1259	05 32 03.4 −67 42 26	05 32 02.6 −67 42 28	5	05 31 56.3 −67 42 19	41	
05329−6709	05 32 51.9 −67 06 52	05 32 51.1 −67 06 56	6	05 32 51.1 −67 06 54	5	
HV5933	05 33 26.9 −67 04 14	05 33 26.5 −67 04 21	7			
05348−7024	05 34 16.1 −70 22 53	05 34 15.6 −70 22 57	5			
HV2700	05 35 19.0 −67 02 20	05 35 21.3 −67 02 43	27			b
05355−6657	05 35 28.3 −66 56 03	05 35 27.6 −66 56 06	5			
05360−6648	05 36 01.3 −66 46 40	05 35 59.5 −66 46 41	11	05 36 01.2 −66 46 38	2	
05433−6728	05 43 10.9 −67 27 28	05 43 11.6 −67 27 43	16			b
05506−7053	05 50 08.7 −70 53 12	05 49 57.7 −70 53 16	54			
05558−7000	05 55 21.1 −70 00 03	05 55 20.8 −70 00 05	2			

a: NIR position determined from SAAO *K* scan (accuracy ~10 arcsec).
b: *IRAS* position taken from Reid et al. (1990).

Table 3. Sources which are not detected or have uncertain counterparts.

Name	IRAS source RA (J2000)	IRAS source DEC (J2000)	$F_{12\mu m}$ (Jy)	$F_{25\mu m}$ (Jy)	possible counterpart RA (J2000)	possible counterpart DEC (J2000)	K (mag)	comment
04518−6852	04 51 39.8	−68 47 29	0.37	0.22				1
HV12501	04 55 39.4	−69 31 22	0.44	0.44	04 55 40.5	−69 26 42	6.8	2
04588−6811	04 58 41.0	−68 07 14	0.30	0.33	04 58 39.4	−68 07 07	13.7	3
05073−6752	05 07 13.9	−67 48 54	0.22	0.44	05 07 12.5	−67 48 47	13.9	1,4
TRM133	05 08 01.0	−65 38 41	0.17	0.22	05 08 08.0	−65 38 52		1,5
05110−6616	05 11 10.8	−66 13 03	0.19	0.33			>14.0	
05150−6942	05 14 40.2	−69 39 20	0.30	0.44	05 14 48.7	−69 39 44	8.25	
05242−6748	05 24 08.2	−67 45 42	0.19	0.22	05 24 08.3	−67 45 48	13.5	6
TRM096	05 26 54.6	−66 21 04	0.12	0.08			>12.5	7
05278−6942	05 27 23.2	−69 39 44	0.37	0.44				1,8
TRM045	05 28 16.3	−67 20 55	0.13	—	05 28 19.1	−67 20 19	>12.5	9
LI-LMC1116	05 28 41.9	−67 28 57	0.12	0.18			>12.5	7
TRM103	05 29 59.7	−65 49 57	0.14	0.23				1
05346−6949	05 34 14.2	−69 47 21	7.40	21.09	05 34 13.7	−69 47 29	>15.5	10
05522−7120	05 51 32.0	−71 19 34	0.19	0.22			>15	
05540−6533	05 54 08.6	−65 33 11	0.30	0.22	05 54 07.6	−65 33 35	16.2	
05568−6753	05 56 38.8	−67 53 40	0.33	0.44	05 56 42.6	−67 53 20	10.8	
05588−6944	05 58 24.8	−69 44 25	0.19	0.56	05 58 25.8	−69 44 28	13.7	

1. Observed with too small an IRAC-2 field (1 arcmin).
2. The *IRAS* position falls near a group of four stars, one of which is HV 12501 (one of the others is classified as A3Ib); either of the four could be the counterpart. On the ESO *R* plate there is a suggestion of nebulosity around the group, and the *IRAS* emission could well be associated with it rather than one of the individual stars.
3. There is a faint, red source at $\alpha = 04^h58^m47^s$, $\delta = -68°07'15''$ which could also be the counterpart. However, the field is very crowded.
4. There is an additional faint, red source in the field which could be identified as the counterpart. However, the *IRAS* source is close to the edge of the 1-arcmin IRAC field. The near-infrared counterpart was detected by Reid (1991) and its position is listed in the table.
5. The IRAC-2 field for TRM133 was centred at the stellar position given by Reid et al. (1990) which puts the *IRAS* position in fact outside the 1-arcmin IRAC-2 field. The near-infrared counterpart was detected by Reid (1991) and its position is listed in the table.
6. There is a star at the correct position, but the star is not obviously red.
7. Not observed with IRAC-2.
8. The field is extremely crowded and a faint counterpart could have been missed.
9. The counterpart was detected by Reid (1991). Scanning at SAAO did not recover the infrared source. Since we estimate the detection limit for scanning to be around $K = 12.5$, whereas Reid detected the counterpart at $K = 11.17$, we believe that the source is variable. The listed position is from Reid.
10. The counterpart was detected by Elias et al. (1986) in the mid-infrared. However, they found it to be very faint in the near-infrared ($K = 16$) and it may have been below our detection limit. The luminosity indicates that it is a supergiant.

ESO *R* plate; it also shows no evidence for variability. We suggest that it could be an H II region. One object (TRM045) we could not confirm, probably because of source variability.

The sources that were not detected are listed in Table 3. In some cases there are possible counterparts, which are not particularly red in the near-infrared. There are several possible reasons for non-detections. (i) The objects lie outside the observed field. This is possible for a number of sources which were imaged with a 1-arcmin field. (ii) The *IRAS* source is non-stellar (or non-existent). (iii) The star associated with the *IRAS* source is neither intrinsically red nor significantly reddened. This could be the case for post-AGB stars having a detached envelope, although the *IRAS* flux will decrease rapidly after the envelope becomes detached. (iv) The star is so highly reddened that the shell is optically thick at *K*. This is the case for at least one object: 05346 − 6946, which has been detected by Elias, Frogel & Schwering (1986) at 10 μm. Further detections of such highly obscured objects will require imaging at longer wavelengths. The other cases could probably be resolved with 10-μm imaging. Detection of either case (iii) or (iv) would yield important additions to our sample.

In case of possible counterparts, we list the *K*-band magnitudes as derived from IRAC-2. These are uncertain because of the non-photometric conditions. For sources without counterparts that were observed with the large field (so that it is unlikely that the counterpart was outside the observed field) we list an upper limit at *K*. This should be taken with caution: it applies only to a possible highly obscured star in the field. In case (iii) above, the *IRAS* source would be associated with one of the detected stars in the field at considerably brighter magnitudes. For the sources observed with too small a field, no relevant upper limit can be given.

Table 4 lists the magnitudes, where in a few cases small corrections have been applied for confusing sources in the aperture. The *IRAS* flux densities are given in janskys; they

Table 4. Magnitudes and IRAS flux densities.

Name	Magnitudes J	H	K	L	IRAS (Jy) 12	25	60
VV Tuc	8.34	7.36	7.12	6.79	0.52	0.33	
00350−7436	11.49	10.16	9.08	7.76	0.30	0.22	
HV12956	10.96	10.14	9.72	8.88:	0.41	0.44	
04286−6937	(15.8)	13.58	11.61	9.50:	0.22	0.17	
04374−6831	(16.7)	14.27:	12.01	9.28	0.19	0.17	
04407−7000	10.62	9.07	8.23	7.25	0.81	0.67	
04496−6958	12.10	10.19	8.80	7.25	0.37	0.33	
04498−6842	12.62:	11.05	9.94	8.64:	1.18	1.11	
04539−6821	(18.2)	(14.7)	12.19	9.14:	0.19	0.22	
WOH SG071	8.87	7.85	7.44	6.84	0.67	0.67	
04557−6753	(15.9)	13.33	11.34	8.75	0.26	0.22	
HV2255	8.57	7.64	7.34	6.85	0.59	0.44	
05003−6712	12.36	10.96	9.78	8.33:	0.44	0.44	
05009−6616	14.57:	12.51	10.76	8.49:	0.26	0.22	
05099−6740	14.62:	12.85	11.54	–	0.19	0.44	0.8
05112−6755	(17.2)	(15.0)	12.68:	9.43:	0.41	0.33	
05112−6739	–	(15.3)	13.08:	–	0.33	0.17	
LI-LMC0578	–	12.54	10.67	8.35	0.15	–	
05128−6455	13.31	11.69	10.31	8.50:	0.15	0.22	
HV928	8.70	7.58	7.27	7.04	0.26	0.17	
05190−6748	–	–	12.16	8.63	0.34	0.23	
TRM088	–	13.60:	11.39	8.99	0.16	–	
WOH G281	7.23	6.20	5.93	5.66	0.33	0.22	
HD271191	7.77	7.01	6.82	6.46	0.18	–	
HV12793	9.15	8.13	7.80	7.37	0.41	0.22	
HV963	8.92	8.00	7.72	7.26	0.18	0.16	
SP47-14	9.05	8.07	7.78	7.38	0.30	0.22	
05289−6617	12.43	11.43	11.22	–	0.11	0.44	
05291−6700	12.71:	10.98	9.92	8.76	0.07	0.22	
05295−7121	(15.2)	12.89	11.03	8.94:	0.19	0.17	
SP45-34	9.08	8.16	7.88	7.50	0.19	0.22	
SP46-44	8.02	7.20	6.99	6.64	0.26	0.11	
05300−6651	(16.4)	13.85:	11.58	9.01:	0.11	0.11	
05304−6722	8.78	7.99	7.69	7.06	0.48	0.22	
HV12998	9.17	8.09	7.71	7.06	0.37	0.22	
HV990	8.52	7.69	7.47	7.13	0.33	0.22	
WOH SG374	9.97	9.24	8.80	7.82	0.36	0.35	
SP52-1	8.83	7.90	7.65	7.30	0.11	0.17	
LI-LMC1259	11.86	11.02	10.05	8.55	1.48	5.99	
05329−6709	(16.6)	(13.2)	11.65	9.20	0.85	1.83	
HV5933	9.15	8.26	7.95	7.44	0.37	0.22	
05348−7024	–	(19)	(13.8)	–	0.48	0.28	
HV2700	9.34	8.44	8.23	8.01:	0.19	0.11	
05355−6657	8.35	7.47	7.24	6.81	0.33	0.22	
05360−6648	(19)	(16.5)	13.56:	–	0.22	0.22	
05433−6728	12.08	11.02	10.90	–	0.15	0.22	
05506−7053	(20)	(15.0)	12.24:	8.93:	0.63	0.67	
05558−7000	11.80	9.93	8.84	7.46	0.74	0.67	

are not colour-corrected. All near-infrared magnitudes are from the 1993 February SAAO observations, except for LI-LMC0578 which was observed in March and the magnitudes given in brackets which are derived from the IRAC-2 images. The SAAO *JHK* measurements are accurate to better than ± 0.04 mag and the *L* measurements to better than ± 0.06 mag, unless marked with a colon in which case the *JHK* are better than ± 0.1 mag and the *L* better than ± 0.12 mag. In the case where the listed magnitudes are taken from the IRAC-2 data, the sources were too faint for photometric measurements. The IRAC-2 magnitudes are somewhat less reliable (also because no extinction correction could be applied owing to the weather conditions), but at the faint levels the error is dominated by background photon noise rather than calibration uncertainties. One should keep in mind that there are uncertainties in the transformation between the Carter (SAAO) and ESO systems. The *IRAS* data are taken from Schwering & Israel (1990), or from Reid et al. (1990).

05329 − 6709, one of the reddest objects in the sample, appears strongly variable: the IRAC observations one month earlier indicated that it was more than 1 mag brighter at *K*. Although the conditions during the IRAC observations were not photometric, this cannot explain such a large difference as the standards varied by only 0.3 mag.

5 SOURCE CLASSIFICATION AND SAMPLE DEFINITION

5.1 Present sample

Fig. 2 shows the *J*–*H*, *H*–*K* diagram for the detected sources. This diagram gives a clear separation between (non-variable) M giants and Miras (Feast, Whitelock & Carter 1990). (The term 'M giants' is used here for those red giant branch (RGB) and AGB M stars that are not undergoing strong Mira pulsations.) The bottom panel shows an enlargement of part of the top panel; the boxes indicate the colour distribution of Galactic Miras and carbon stars (Feast et al. 1982; Bessell et al. 1989a; Whitelock et al. 1994), M dwarfs (Tinney, Mould & Reid 1993), M giants (Feast et al. 1990) and LMC M-type supergiants (Wood, Bessell & Fox 1983). The colour systems used have been transformed to the Carter system using formulae given by McGregor (1994). Carbon stars tend to have a slightly redder *J*–*H* than (M-type) Miras but otherwise the two groups occupy the same general colour region. Both kinds of star can suffer from circumstellar reddening, which is the reason for the 'open-ended' box. The main confusion comes from supergiants: separating the M giants and Miras from supergiants requires knowledge of the absolute magnitude. A few supergiants with very high circumstellar reddening are known in the Milky Way, so that even for reddened objects confusion between Miras and supergiants still exists.

Most of the stars in our sample separate into two different groups in the figure. One group has colours characteristic of M giants, while the other group shows evidence for high reddening. Fig. 3 shows the colour–magnitude diagrams as a function of the *K* magnitude. It can be seen that the 'blue' group corresponds to the brighter stars at *K*, making an identification with supergiants or foreground M giants likely.

A number of objects are rejected from the sample for various reasons. They are indicated as star symbols in Figs 2 and 3. The following three sources are rejected because of their colour and *K*-magnitude.

LI-LMC1259. This object is located around $(J-H, H-K)=(0.8, 1.0)$ and falls outside any obvious group: this is the object that we previously mentioned (Section 4) might be an H II region or young stellar object.

05433 − 6728 and 05289 − 6617. They appear close to the 'M-giant' clump while being much fainter at *K*. Based on the faint magnitudes, both objects are likely foreground stars and may not be related to the respective *IRAS* source.

There are in addition a number of objects that are likely Galactic (foreground) stars.

WOH G281. This object is a magnitude brighter at *K* than any of the others. From the *VRI* magnitudes, Westerlund et al. (1981) also suspect that it is a foreground star. The 12-μm flux is consistent with photospheric emission.

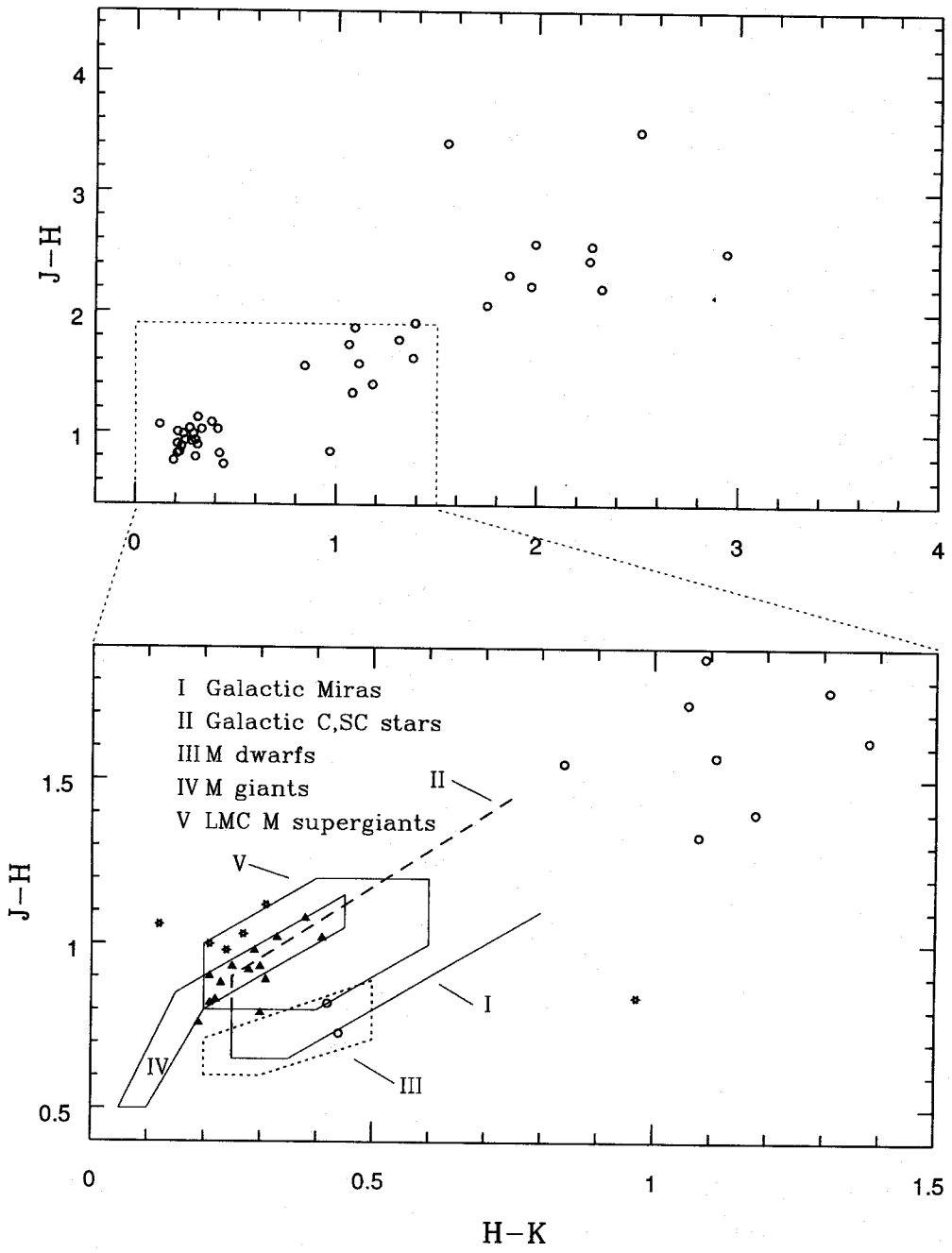

Figure 2. $J-H$ versus $H-K$ for the sources observed at ESO and SAAO. The lower diagram shows an enlargement of the bottom-left corner, indicating where various classes of stars would fall. In the lower diagram, the open circles indicate possible reddened AGB stars, the filled triangles possible M giants or supergiants, and the open star symbols foreground stars.

VV Tuc. The association of the *IRAS* source with this known variable star, together with the very bright magnitudes which would give $M_{bol} = -8.5$ at the distance of the SMC, argues in favour of a foreground star although an identification as supergiant cannot be completely excluded. There are no velocity measurements available.

HV928. Wood & Bessel (1985) find a velocity of about 60 km s^{-1}. It is identical with ZZ Men and is certainly a foreground star.

In the bottom panel of Fig. 3 it can be seen that the 'rejected sources' have on average significantly redder *IRAS* colours than the other stars. The two suggested M giants are faint at 12 μm and may be confused. The two possible foreground Miras, VV Tuc and ZZ Men, are much brighter and their association with the respective *IRAS* source is likely. Velocity measurements would be desirable for VV Tuc to establish its relation to the SMC.

There are three sources for which the colours could be

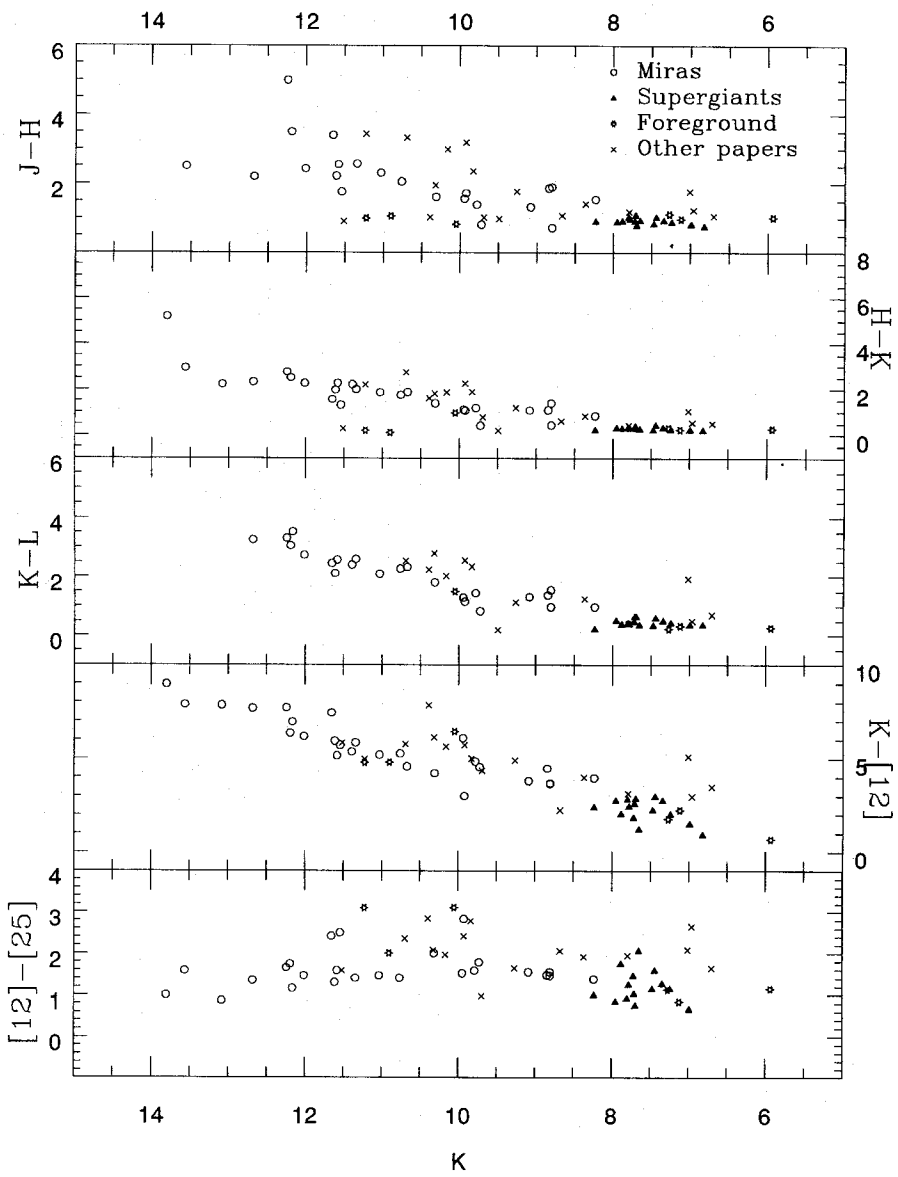

Figure 3. Colour–magnitude diagrams for the stars in the Magellanic Clouds. *IRAS*-detected AGB stars from other papers are also included.

consistent with unreddened Miras or even M dwarfs: 05304 – 6722, WOH SG374 and HV12956. The first object we classify as supergiant, based on the bolometric luminosity. The second is identified with the optical star WOH SG374: Westerlund et al. (1981) classify it as a probable supergiant. The spectral type is M6 which would be unusually late for a supergiant. We find that the bolometric magnitude would be low for an LMC supergiant, but high for a Mira. The lack of reddening is surprising given the strength of the mid-infrared emission. HV12956 is a well-known Harvard variable (e.g. Whitelock et al. 1989) for which the association with the SMC has not been in doubt so far and which is known to be a long-period Mira variable. We later will show that the *IRAS* source is indeed associated with the star. Based on the present data we note the possibility that both sources might be foreground Miras. However, they will be included in the final sample.

For three objects the separation between the *IRAS* source and the near-infrared source is more than 30 arcsec, casting doubt on their association. They are: 05099 – 6740, 05295 – 7121 and 05506 – 7053. In all three cases the near-infrared colours are indicative of significant reddening. Although *IRAS* sources sometimes show such large positional deviations, there is a possibility that these sources have been discovered by accident.

5.2 Previously known stars

In addition to our sample, candidates for *IRAS*-detected AGB stars in the Magellanic Clouds have been reported by Whitelock et al. (1989), Reid (1991) and Wood et al. (1992). 14 objects are listed in Wood et al. (1992) (excluding one which is also in our sample); their sample includes both AGB stars and supergiants. Three of their objects are in the

SMC. There is one additional source in Reid (1991) (excluding the objects already in our sample and one object in common with Wood et al.). Two SMC *IRAS*-Miras are listed by Whitelock et al. (1989) (excluding one already in our sample). Table 5(a) lists the additional objects. The photometry is from the original sources and is in various photometric systems. Especially at J a significant correction between systems is required for red objects (McGregor 1994); the conversion between the L and L' systems is also uncertain.

Three sources listed in Wood et al. are not included in Table 5(a).

04571 – 6954 is identical with the B8Ia star HD 268835, also known as S73 or R66, and is a known S Dor variable (Shore & Sandulaek 1984). Due to its early spectral type, the luminosity is far higher than derived by Wood et al. based on the near-infrared flux.

05244 – 6832 is a very red *IRAS* source with little variability. For this reason Wood et al. suggest that it might be a post-AGB star. However, it is very close to the H II region LHA 120-N 1380 and it is probably not an evolved star.

05325 – 6743 is identical to the well-known H II region LHA 120-N 57A. It also has the *IRAS* colours expected for an H II region.

Furthermore, Hughes & Wood (1990) have presented a catalogue of optically visible long-period variables (LPVs) in the LMC: we have correlated our *IRAS* source list with this catalogue which gave three further possible detections. They are listed in Table 5(b). The first column lists the name as used in Hughes & Wood. The last two columns list optical identifications as well as spectral type. The first two objects have also been classified as (super)giants, but the periods and magnitudes are consistent with LMC Miras.

The additional sources in Tables 5(a) and (b) are indicated in Fig. 3 by the crosses, where we have corrected the magnitudes to the Carter system. Fig. 4 shows the $J-H$ versus $H-K$ diagram for these sources. The filled circles indicate the sources for which Wood et al. (1992) detect OH emission at velocities corresponding to the LMC. (One of these is not in Table 5a because it is also in our sample.) There are a few sources for which the classification is not clear; in the tables these are indicated by a question mark.

01039 – 7305 and 05216 – 675 are brighter at J than expected from the $H-K$ colours, which may indicate a blue underlying star. The two objects are very similar: both have very red *IRAS* colours and show only small-amplitude variations. However, 05216 – 6735 is very bright and is classified as a supergiant, whereas 01039 – 7305 is much fainter and could be a post-AGB star.

00477 – 7343 could be a foreground star, based on its *JHK* colours, but it is also one of the brightest *IRAS* sources in the sample: the *IRAS* colours are characteristic of an H II region. The *IRAS* source is near a supernova remnant (0047 – 73.5) which together with the *IRAS* colours makes an association with a star-forming region likely.

0510004 – 692755 has a very short period. It also does not

Table 5. (a) MC *IRAS*-AGB stars from other sources.

name	J	H	K	L	L′	12	25	60	P	comment	spectral type
Whitelock et al. 1989 (SMC)											
00483–7347	11.58	9.97	8.79	7.38	–	0.65	0.48		>1000		
00554–7351	(15)	12.98	10.85	8.47	–	0.37	0.20		800		
Reid 1991 (LMC)											
TRM045	16.18	13.36	11.17	–	–	0.13	–				
Wood et al. 1992 (SMC)											
00477–7343	10.59	9.69	9.49	–	9.29	<0.40	1.12	10.4		non-Mira?	
00521–7054	13.86	12.53	11.23	–	9.07	0.28	0.80	1.02			
01039–7305	14.68	13.54	11.76	–	9.31	0.27	0.95	3.7		non-Mira?	
Wood et al. 1992 (LMC)											
04509–6922	10.46	9.20	8.35	–	7.11	0.74	1.00		1290		
04516–6902	11.59	9.89	8.86	–	8.05	0.63	0.78		1090		
04530–6916	13.76	11.70	9.79	–	7.49	2.00	4.97		1260		
04545–7000	16.34	13.45	10.64	–	8.16	0.44	0.89		1270		
04553–6825	9.64	8.06	6.99	–	5.08	7.07	11.21		930	**WOH G064**	M7.5
05216–6753	12.84	12.02	10.38	–	8.16	3.91	12.39			non-Mira?	
05247–6941	8.62	7.49	6.96	–	6.46	1.04	2.77			**WOH SG264**	M2
05261–6614	9.30	8.23	7.79	–	7.38	0.56	0.78				
05294–7104	12.01	10.45	9.24	–	8.12	0.74	0.78		1040		
05298–6957	13.83	12.14	10.29	–	7.53	0.85	1.33		1280		
05389–6922	8.17	7.21	6.70	–	5.99	2.11	2.22			**WOH SG453**	M0.5
05402–6956	14.58	12.02	10.12	–	8.14	0.63	0.89		1390		

Table 5. (b) Known LPVs in the LMC detected by *IRAS*.

name		J	H	K	12	25	P	optical name	spectral type
0453582–690242	LI-LMC 143	10.25	9.29	8.67	0.11	0.17	857	**WOH SG061**	M0
0454257–684856	LI-LMC 153	11.39	10.47	9.68	0.30	0.17	728	**SP 30-6**	M8
0510004–692755	LI-LMC 530	12.63	11.81	11.51	0.22	0.22	169		?

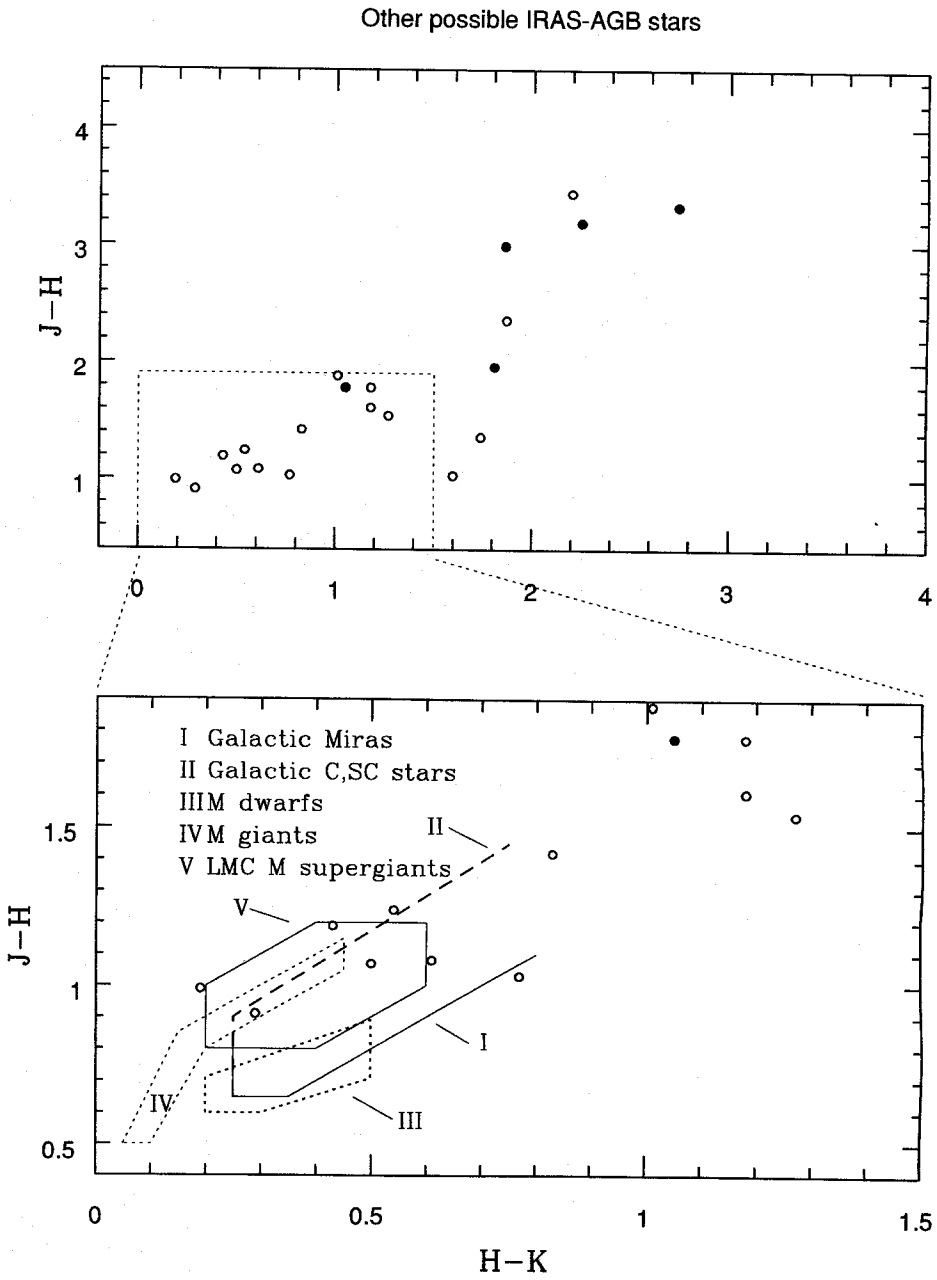

Figure 4. $J-H$ versus $H-K$ for the *IRAS*-detected AGB stars from other papers. The filled circles indicate the stars for which Wood et al. (1992) detected OH emission.

show noticeable reddening and the *IRAS* detection is therefore surprising. Further observations to confirm its association with the *IRAS* source would be desirable.

Separating supergiants from AGB stars requires knowledge of the luminosity. We will therefore first discuss the method used to determine the bolometric magnitude, before returning to the problem of classification.

5.3 Bolometric magnitudes

We calculate the bolometric magnitudes from the available infrared photometry, by integrating under a spline curve fitted to the J, H, K, L, 12- and 25-μm fluxes as a function of frequency. At the blue end, we extrapolate a line joining the K flux to a point lying mid-way between the J and the H data points. At the other end, we assume zero flux at zero frequency. The procedure is discussed in detail in Whitelock et al. (1994) and it is better than a blackbody fit for sources with a significant fraction of the energy arising longward of L. Whitelock et al. show that the difference with blackbody fits is about 0.05 mag when $J-K$ is between 1.1 and 1.8. The procedure underestimates the luminosity for extreme *IRAS* sources where a substantial fraction of the energy comes out longward of 25 μm. The reddest sources may have $F_{60\,\mu m}=3F_{25\,\mu m}$, leading to an underestimation by 25–50 per

cent. It is, however, unlikely that AGB stars with such colours would have been discovered in the LMC, because for AGB stars the 12-μm flux would be below the detection limit. Very red supergiants may be affected.

The accuracy of the derived bolometric magnitudes is limited by several effects. First, the measurement errors, although negligible for supergiants, are significant for the fainter AGB stars. For very red sources the total luminosity is dominated by the 25-μm flux, which for our sample is the most uncertain data point. An error of a magnitude for such a source could lead to an uncertainty of almost a factor of 2 in the luminosity. Secondly, there are strong water-vapour absorption bands for oxygen-rich M stars in the near-infrared, which fall between the standard *JHKL* bands and are difficult to account for in the flux determination. The overall effect of these results in the bolometric magnitudes being overestimated by 0.1 to 0.2 mag in optical Miras (Robertson & Feast 1981). The effect will be less in stars with thick dust shells. Thirdly, variability will affect the bolometric magnitudes. The sources from Wood et al. have good period coverage, but the others have only been observed once. The average bolometric magnitude may differ from the ones derived here by typically a few tenths of a magnitude although larger differences are possible for the sources with largest amplitudes. Variability will especially affect the AGB stars: supergiants tend to have lower amplitudes.

For the sources taken from the literature we have redetermined m_{bol} using the present method: the agreement with the previously determined values is in general good to within 0.1 mag. In two cases the *IRAS* colours were so red that the present method would miss a significant part of the bolometric flux. For these objects (05216−6753 and 00477−7343) a literature value will be quoted instead. 00477−7343 has a large discontinuity between the near-infrared and *IRAS* colours, so that any fit is poorly constrained.

For conversion to luminosity, we assume a distance modulus for the LMC of $(m-M)_0=18.47\pm0.15$ and for the SMC of $(m-M)_0=18.78$ (Feast & Walker 1987), corresponding to 49 and 57 kpc respectively.

Table 6. Bolometric magnitudes for supergiants and sources with uncertain classification.

Name	m_{bol}	K−[12]
supergiants		
04530−6916	10.7	7.09
WOH G064	9.2	5.61
WOH SG071	10.5	3.42
HV2255	10.3	3.12
HD271191	9.3	1.33
05216−6753	10.07[a]	5.07
HV12793	10.9	3.09
WOH SG264	10.1	3.56
05261−6614	10.9	3.64
HV963	10.8	2.23
SP47-14	10.9	2.81
SP45-34	10.9	2.50
SP46-44	9.7	1.72
05304−6722	10.4	3.09
HV12998	10.9	2.91
HV990	10.2	2.57
SP52-1	10.7	1.72
HV5933	10.9	3.15
HV2700	11.1	2.68
05355−6657	10.1	2.34
WOH SG453	9.7	3.94
uncertain		
00477−7343	11.8[a]	6.45
01039−7305	12.7	6.93
0510004−692755	13.2	6.29

[a] m_{bol} taken from Wood et al. (1992).

5.4 Supergiants and peculiar sources

We will now attempt to distinguish between supergiants and Miras, using several criteria. The clearest indicator is luminosity: although there is a possible area of overlap in luminosity, supergiants are in general much brighter than AGB stars and one could classify objects with luminosities above the classical AGB limit of $M_{bol}=-7.1$ as supergiants. Blöcker & Schönberner (1991) have shown that in some cases AGB stars can attain luminosities higher than the classical limit and this criterion should therefore not be applied too strictly. For sources with only one observation, a Mira that happened to be near maximum may also have $M_{bol}<-7.1$. We have chosen to classify all objects with $M_{bol}<-8.0$ as supergiants. Two further criteria are used. Objects with $M_{bol}<-7.1$ and small-amplitude variability typical of supergiants (<0.5 mag at K) are classified as such. This information is available for the sources in Wood et al. (1992). Finally, objects with $M_{bol}<-7.1$ and colours within region IV of Fig. 2 are classified as supergiants. We added 04530−6916 to the list because it is very close to the chosen M_{bol} limit and its luminosity was probably underestimated because of the very red *IRAS* colours.

We note that it is possible that some objects are still misclassified. The best way to classify these objects would be through abundance determination, in particular s-process elements or lithium (Smith & Lambert 1989, 1990) which are dredged up in luminous AGB stars but not in supergiants. Smith et al. (1994) found for a sample of 112 optically visible red giants that lithium is mainly found in stars within a narrow luminosity range ($-7.2\lesssim M_{bol}\lesssim-6.0$), in agreement with the classical limits. It is not known whether this conclusion can be extended to obscured, mass-losing stars: abundance studies would be desirable for the present sample.

Table 6 lists the bolometric magnitudes and the $K-[12]$ colour for the 20 objects classified as supergiants. In addition, three objects are listed for which the classification is not clear, for reasons mentioned in Section 5.2. Fig. 5 shows the spectral energy distribution for the stars we classify as supergiants and for the objects with uncertain classification. For a blackbody spectrum with an effective temperature of 2500 K we expect $K-[12]=0.76$. A blackbody of this temperature is illustrated in one of the spectra of Fig. 5: HD 271191, for which the 12-μm flux appears to be dominated by photospheric emission. In general a blackbody is not expected to give a good fit to these late-type stars: the near-infrared colours are modified by strong molecular absorption features, particularly H_2O and CO, as well as H^- (Bessell et al. 1989b). The exact contribution of dust to the 12-μm flux is therefore uncertain. However, most of the

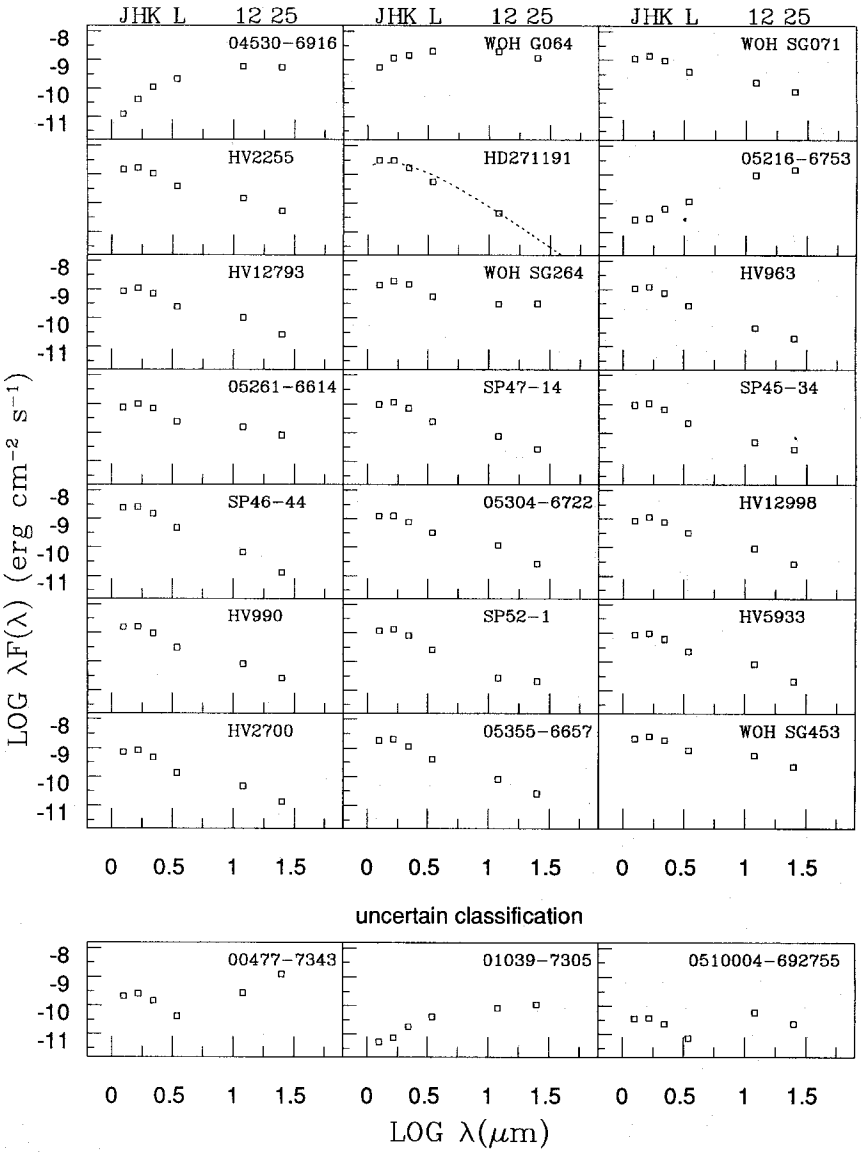

Figure 5. Spectral energy distribution for 20 supergiants and three objects with uncertain classification in the Magellanic Clouds. The curve in one spectrum shows a blackbody with a temperature of 2500 K.

supergiants exhibit a small but clear excess in the *IRAS* bands, over an extrapolation from the near-infrared colours, indicating mass loss. The mass-loss rates appear not to be very high since the near-infrared colours are in most cases not noticeably reddened. From the $K-[12]$ colours we estimate $\dot{M} < 10^{-8}$ $M_\odot$ yr^{-1} (see Section 8.2, but allowing for the fact that V_{exp} may be several times larger for supergiants than for AGB stars). Two of the supergiants exhibit significant reddening indicative of much larger mass-loss rates: 04530 – 6916 and 05216 – 6753. The last object clearly shows the excess flux at *J* mentioned in Section 5.2.

WOH G064 shows a peculiar, flat energy distribution. This source is also the most luminous object in our sample with $M_{bol} = -9.3$. The optical counterpart, discovered by Westerlund et al. (1981), has a very late spectral type of M7.5 (Elias et al. 1986). The flat energy distribution may indicate binarity or asphericity. The luminosity of this object is close to the upper limit where red supergiants occur (e.g. Chiosi & Maeder 1986, their fig. 3), implying a progenitor mass of close to 50 $M_\odot$. It is surprising that such a massive star has evolved to such a late type. This is one of the most interesting sources in the sample.

Two of the sources with uncertain classification show a very large excess in the *IRAS* bands without significant reddening in the near-infrared. The association of star and *IRAS* source is therefore in doubt. For the first source, 00477 – 7343, the *IRAS* source is probably an H II region. 01039 – 7305 is classified as uncertain because of the excess emission at *J*.

6 AGB STARS

There are 34 sources in the LMC and five in the SMC that are good candidates for AGB stars. The spectral energy distributions of these sources are shown in Fig. 6. Most objects are significantly reddened even in the near-infrared.

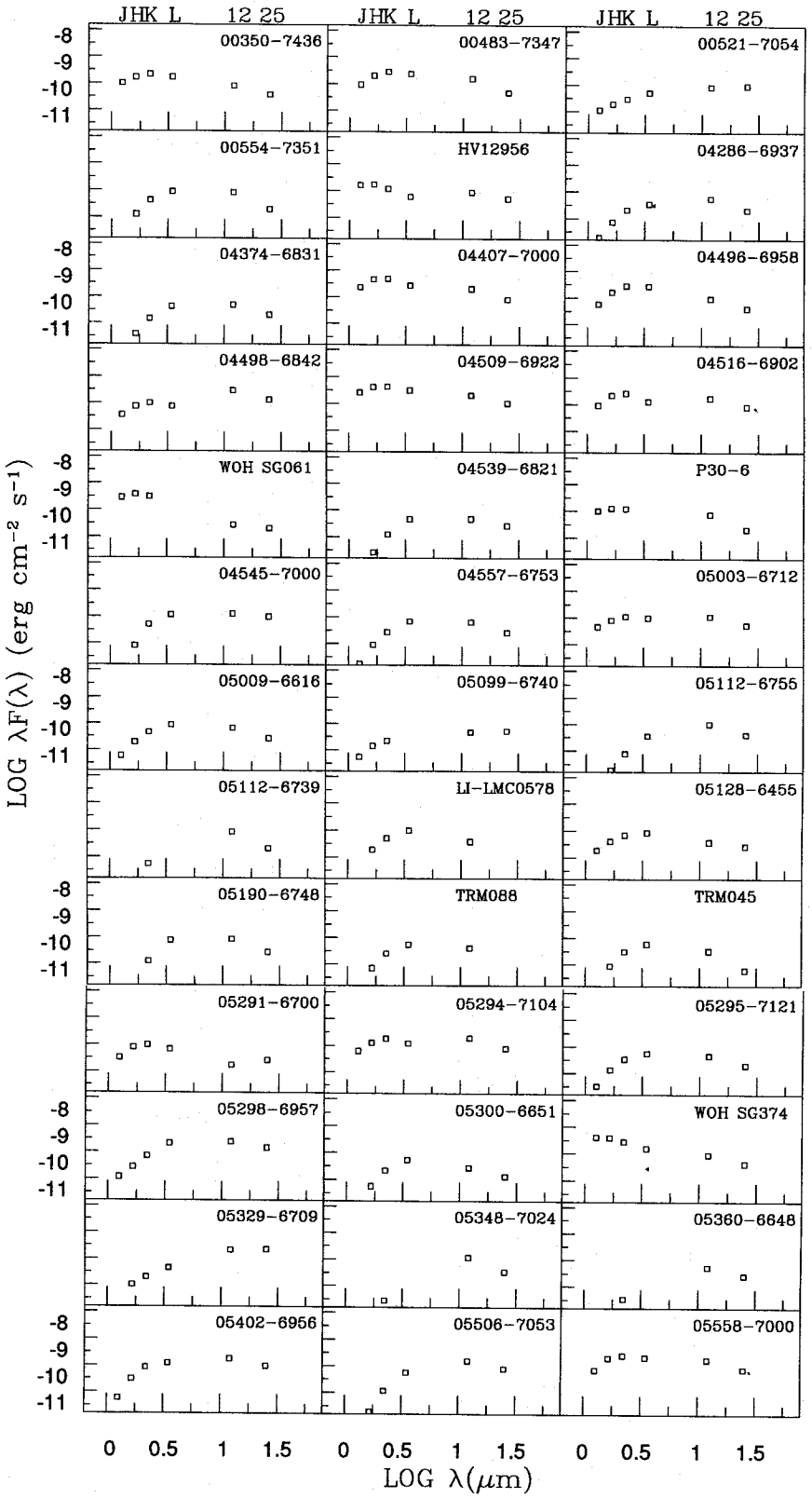

Figure 6. Spectral energy distribution for candidate AGB stars in the Magellanic Clouds.

A few cases have *IRAS* flux densities higher than expected from the near-infrared data (especially 04498 – 6842 and 05294 – 7104) but this may be due to variability. The sources are listed in Table 7: we give the bolometric magnitudes, calculated as described in the previous subsection, the $K-[12]$ colour which is an indicator for the mass-loss rate (Whitelock et al. 1994), λ_{10} which is the effective heating wavelength of the incident radiation, as defined by Jura (1987; see also Whitelock et al. 1994), and the bolometric luminosity.

The derived luminosities are in almost all cases above 10^4 $L_\odot$. It is clear that only the upper part of the luminosity function of Magellanic Cloud of AGB stars is detected. The IRAC-2 survey would have found fainter sources if the circumstellar extinction were not very high but lower-luminosity objects with moderate circumstellar shells were evidently not detected by *IRAS*. This might be anticipated since the (present) luminous sources are already close to the detection limit in the *IRAS* data base. Our results show that there are some high-luminosity AGB stars in the LMC which experience heavy mass loss, although with the present data we cannot decide whether lower-luminosity stars reach the same mass-loss rates and become similarly obscured. It is possible that the recently started near-infrared sky surveys, such as the DENIS project, will find such objects.

The classical upper limit for the luminosity of an AGB star, derived from the Chandrasekhar limit for the mass of the core together with luminosity–core-mass relation, corresponds to $\log L_\star = 4.75$. Blöcker & Schönberner (1991) have recently shown that highly convective, massive AGB stars can evolve to luminosities well above those predicted by the luminosity–core-mass relation, i.e. $\log L_\star > 4.75$, during envelope burning. The luminosities in our sample do not extend above the classical limit. However, it is possible that overluminous objects would be misclassified as supergiants since it is difficult to separate the two groups. In fact, there are theoretical indications that the core mass of AGB stars does not grow beyond 0.9–1.2 $M_\odot$ (Han et al. 1994). Observationally this is difficult to confirm: the only evidence comes from the masses of white dwarfs in young clusters (Weideman 1987; Vassiliadis & Wood 1993) which also do not extend to the Chandrasekhar mass. If this reduced upper mass limit were true, the actual 'classical' limit for the luminosity of AGB stars would be closer to $M_{bol} = -6.9$ in which case some objects in our sample would be overluminous. We conclude that it will be very difficult to prove or disprove the Blöcker & Schönberner scenario based on the present sample.

Table 7. Candidate AGB stars.

Name	m_{bol}	K–[12]	λ_{10}	$\log L_\star$ [$L_\odot$]
00350–7436	12.1	4.28	0.69	4.6
00483–7347	11.6	4.66	0.77	4.7
00521–7054	12.7	6.40	1.44	4.3
00554–7351	12.7	6.02	0.98	4.3
HV12956	12.1	5.04	0.75	4.6
04286–6937	13.3	6.34	1.10	4.0
04374–6831	13.4	6.58	1.07	3.9
04407–7000	11.3	4.34	0.71	4.8
04496–6958	11.8	4.12	0.65	4.5
04498–6842	11.6	6.52	1.24	4.7
04509–6922	11.3	4.49	0.78	4.8
04516–6902	11.8	4.81	0.93	4.6
WOH SG061	12.0	2.74	0.38	4.5
04539–6821	13.3	6.81	1.11	4.0
SP 30-6	12.6	4.63	0.69	4.2
04545–7000	12.3	6.28	1.27	4.4
04557–6753	13.0	6.25	1.01	4.1
05003–6712	12.3	5.31	0.95	4.4
05009–6616	12.8	5.67	0.93	4.1
05099–6740	13.2	6.27	1.41	4.0
05112–6755	12.8	8.08	1.25	4.2
05112–6739	13.2	8.11	1.19	4.0
LI-LMC0578	13.1	4.98	0.70	4.0
05128–6455	13.0	4.76	0.83	4.1
05190–6748	12.8	7.30	1.05	4.1
TRM088	13.4	5.77	0.86	3.9
TRM045	13.6	5.33	0.85	3.8
05291–6700	13.1	3.55	0.72	4.0
05294–7104	11.8	5.34	1.04	4.5
05295–7121	13.2	5.60	0.95	4.0
05298–6957	11.7	6.61	1.27	4.6
05300–6651	13.6	5.55	0.88	3.8
WOH SG374	11.3	4.26	0.49	4.8
05329–6709	11.7	8.01	1.52	4.6
05348–7024	12.7	9.21	1.17	4.2
05360–6648	13.4	8.34	1.29	3.9
05402–6956	12.0	6.10	1.21	4.5
05506–7053	12.2	8.16	1.30	4.4
05558–7000	11.6	4.91	0.85	4.7

7 10-μm PHOTOMETRY AND ENVELOPE CHEMISTRY

7.1 TIMMI imaging

AGB stars can have either carbon-rich or oxygen-rich envelopes, depending on their initial C/O ratio and how much carbon has been dredged up following thermal pulses. The chances of an AGB star becoming a carbon star increase with diminishing envelope mass. The mass-loss process is crucial: if high mass-loss rates occur they will reduce the time available for dredge-up and increase the likelihood of the AGB star ending up oxygen-rich. The mass-loss efficiency probably depends on both the progenitor mass and the metallicity.

For our obscured stars the composition can in principle be derived from the mid-infrared emission from the circumstellar envelope. In the case of a carbon-rich shell, we expect an emission feature at 11.3 μm caused by SiC grain mantles. An oxygen-rich shell would lead to a silicate feature (in either emission or absorption) at 9.8 μm. This last feature is broad and can be very strong; if present it will also dominate the emission at 11.3 μm. However, the stars are too faint for mid-infrared aperture photometry and require imaging through a 10-μm camera.

We selected six sources from the objects tentatively classified as AGB stars for 10-μm photometry using the TIMMI camera (Käufl et al. 1992). To separate the features, we observed through three filters: standard N and two narrow-band filters centred at the features (see Section 3.3). The results are shown in Table 8. Listed are: the observed magnitudes, the corresponding N-band (10-μm) flux, the *IRAS* 12- and 25-μm fluxes, A_{10} (indicating the strength of the silicate feature), the K magnitude and the $H-K$ colour. The last two are taken from observations at SAAO carried out in the first week of 1993 November, only four weeks before the

Table 8. TIMMI results.

source	N	±	magnitudes 9.8μm	±	11.3μm	±	flux N (Jy)	IRAS (Jy) F_{12}	F_{25}	K	H−K	A_{10}
HV12956	5.78	0.04	4.77	0.07	4.98	0.04	0.18	0.35	0.42	9.95	0.44	1.9
04407−7000	4.76	0.02	3.89	0.04	4.03	0.04	0.46	0.81	0.67	8.84	1.53	1.6
04498−6842	3.67	0.02	3.17	0.05	3.14	0.03	1.26	1.18	1.11	9.94	0.65	0.88
05112−6755	5.56	0.05	5.32	0.19	5.56	0.06	0.22	0.41	0.33	13.21	1.9	0.36
05295−7121	7.17	0.10					0.050	0.19	0.17	10.49	1.82	
05329−6709	3.91	0.02	3.93	0.08	3.52	0.03	1.01	0.85	1.83	9.65	2.34	-0.16

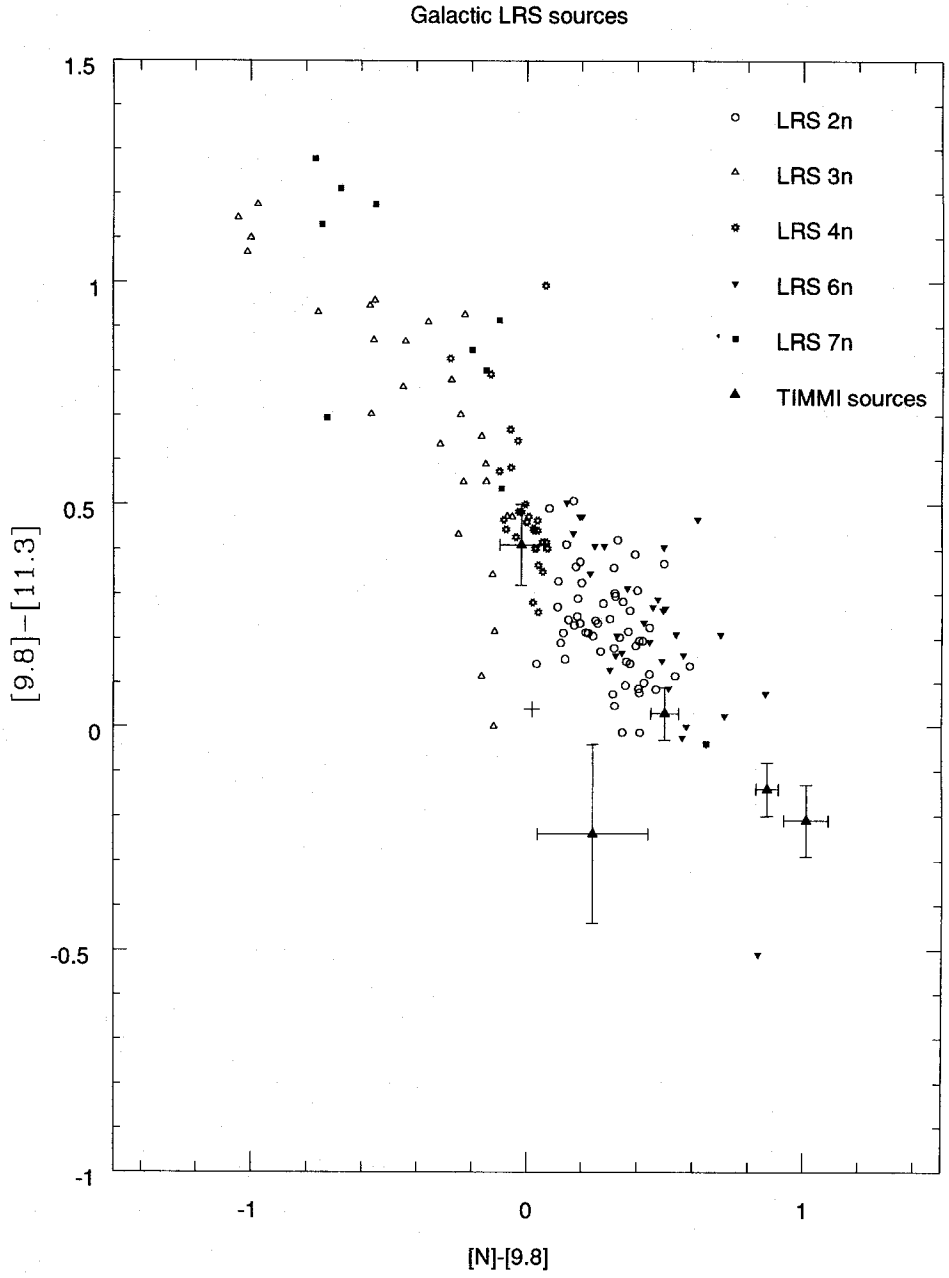

Figure 7. Mid-infrared colours for Galactic AGB stars taken from the *IRAS* LRS data base. The cross indicates our calibrator γ Ret. The triangles with error bars represent the TIMMI data for Magellanic Cloud stars.

TIMMI observations, thus minimizing the effects of source variability. The *N*-band magnitudes are converted to fluxes assuming that $N=0$ corresponds to 37.0 Jy. The measured magnitudes are, in most cases, significantly different from those derived from *IRAS* fluxes. This may in part be due to the intrinsic uncertainties in the *IRAS* fluxes (caused by the large beamsize and the background subtraction) which can be large for sources close to the *IRAS* detection limit in crowded areas. However, the difference in filters (*N*-band versus *IRAS* 12-μm) as well as source variability may also make a contribution. For the largest-amplitude AGB stars, the 12-μm flux can vary by as much as a magnitude (Le Bertre 1993). The results suggest that the Schwering & Israel catalogue should be used with care for such sources. In the case of 05295 – 7121, the poor agreement of the magnitudes, plus the fact that the position of the *IRAS* source is almost 45 arcsec removed from the near-infrared star, suggests that the two are not related, and that the discovery of the AGB stars was fortuitous. This source could not be observed in the two narrow bands because of its faintness.

Of the five sources with sufficient measurements, three are much fainter in *N* than in the narrow bands. Two of these are brightest in the silicate band, and appear to show strong silicate emission. The third source is somewhat brighter at 11.3 μm which makes it difficult to classify. Of the two remaining sources, 05112 – 6755 is tentatively classified as having weak silicate emission, but the uncertainty on the magnitude is too large to be sure. Finally, 05329 – 6709 is brightest in the 11.3-μm band and either could show SiC emission or could be partly self-absorbed silicate: when the feature begins to be absorbed between 9 and 10 μm it can still be slightly in emission longward of 10 μm.

The classification can be secured by comparing with spectra of Galactic AGB stars. We have extracted from the *IRAS* Low Resolution Spectra (LRS) data base (maintained in STARCAT) a random sample of spectra from classes exhibited by AGB stars. We subsequently multiplied the spectra with the passbands of the three filters; the same procedure was applied to the LRS spectrum of γ Ret to calibrate the results. The resulting colours $[N]-[9.8]$ versus $[9.8]-[11.3]$ are plotted in Fig. 7 for the various classes. We remind the reader of the following definitions: class $2n$ – blue continuum with silicate emission; $3n$ – blue continuum with silicate absorption; $4n$ – blue continuum with SiC emission; $6n$ – red continuum with silicate emission; $7n$ – red continuum with silicate absorption. The index n indicates the strength of the feature. In a few cases the spectra were obviously misclassified and have been reclassified.

The figure shows that the stars with SiC emission occupy a well-defined region as defined by these colours. The silicate stars show a very large scatter, because the silicate feature is much stronger than the SiC band and can be in either emission or absorption. Although a small number of the silicate stars coincide with the SiC stars, the chosen filters allow one to identify oxygen stars with confidence; however, a carbon star would not have unique colours. The five stars observed with TIMMI in all three bands are plotted with error bars. Two conclusions can be drawn: four out of the five stars definitely fall in the oxygen-rich category, and two sources have an unusually large ratio of [9.8] to [11.3] and of [9.8] to *N*, which could be indicative of a very strong silicate emission feature. One of the two, HV 12956, is a possible Galactic foreground object. There are a number of stars with similar colours in the LRS data base; they are invariably classified as '69' and are faint, compared with the other LRS sources, with generally $f_{12}\leq 20$ Jy. The continuum underneath the silicate feature is not detected in these stars, which is the reason for the '69' classification. It is possible that these MC stars show a similar large silicate-to-continuum ratio, albeit at a much higher absolute flux. Alternatively, it is possible that the silicate feature is narrower in the Magellanic Clouds than in the Galaxy. 05112 – 6755 also has an unusual position in the diagram, but the error bars are large. For 05329 – 6709 the diagram is inconclusive. Although it is positioned right in the centre of the distribution of carbon-rich stars (class $4n$), oxygen-rich stars can be found in the same region too.

Wood et al. (1992) also prove that several of their AGB stars in the LMC are oxygen-rich, based on the discovery of OH maser emission. Their sources are generally more luminous than the present sample. 05329 – 6709 is also in their sample, and they detect OH maser emission from this source. Self-absorbed silicate emission is a common feature of heavily obscured OH/IR stars and its mid-infrared colours are thus consistent with an OH detection. This supports its classification as an oxygen-rich source. (However, it is possible that the OH detection refers to a different source, since there are other *IRAS* sources within the Parkes primary beam, e.g. TRM58.) We conclude that at least four and probably all five stars observed with TIMMI are oxygen-rich.

The strength of the 9.8-μm silicate feature is quantified by Schutte & Tielens (1989) through the parameter A_{10}, which is the magnitude excess at 9.8 μm (F_{obs}) compared with a continuum (F_c) fitted between two narrow-band filters at 12.5 and 8.7 μm:

$$A_{10}=2.5\log(F_{obs}/F_c). \qquad (1)$$

A_{10} can be estimated for our sources from the $[N]-[9.8]$ colour. To show this, Fig. 8(a) relates the two quantities for a number of randomly selected LRS spectra with classification $2n$ or $6n$ (i.e. silicate in emission). A reasonable correlation is found up to $A_{10}=1.2$:

$$A_{10}=2([N]-[9.8])-0.12 \qquad \pm 0.15. \qquad (2)$$

The resulting values are listed in Table 8. Fig. 5 in Schutte & Tielens shows the predicted and observed relations between A_{10} and the $[3.8]-[12.5]$ colour temperature for a number of Galactic sources. We can compare their predictions with our sources by converting $K-[N]$ to a colour temperature, which for our sources is in the range 600–1000 K. The comparison is shown in Fig. 8(b), where the triangles present the data for Galactic stars from Schutte & Tielens, and the filled circles are the LMC stars. The line illustrates one model with a dust formation temperature of 750 K, taken from Schutte & Tielens, their fig. 5(a). They present a series of models which cover the observational points. Four of our sources fall above the models; the remaining one (05329 – 6709) is in good agreement. The two bluest LMC stars appear to have larger A_{10} than Galactic AGB stars of similar colour temperature, whereas the two reddest LMC

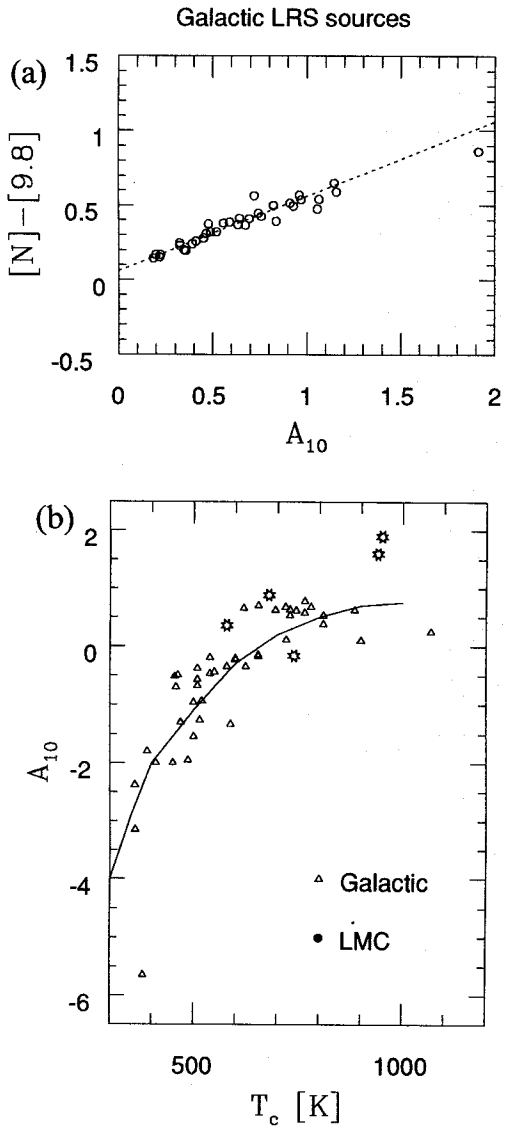

Figure 8. (a) Relation between A_{10} and the $N-[9.8]$ colour for Galactic AGB stars, derived from spectra taken from the *IRAS* LRS data base. (b) Relation between IR colour temperature T_c and A_{10}. Triangles indicate Galactic stars from Schutte & Tielens (1989), and the star symbols indicate LMC stars. The tracks are a representative model from Schutte & Tielens.

stars lie near the upper envelope for the Galactic stars. Based on the present sample, it appears possible that the emission strength of the silicate feature tends to be larger in the LMC than in the Galaxy. More mid-infrared observations of LMC stars will be necessary to confirm this. A stronger silicate feature can be caused by a *lower* silicate optical depth, since the feature already peaks at $\tau \approx 0.2$ (Groenewegen, private communication). Self-absorption reduces the strength at larger optical depth. The indication that the silicate feature is stronger in the LMC could thus be consistent with expectations based on the LMC metallicity.

We find that the present sample shows silicate features indicative of intermediate-to-low mass-loss rates, with $\tau_{9.8} < 3$.

7.2 Separating oxygen-rich from carbon-rich stars

A large number of AGB stars have been found in our Galaxy from follow-up studies of *IRAS* sources. Fouqué et al. (1992) and Guglielmo et al. (1994) observed more than 1300 *IRAS* sources and found in this way over 600 AGB stars. The stars can be easily separated into carbon stars and oxygen stars using the LRS classification. We have used this sample for comparison with the Magellanic Cloud stars.

Fig. 9 shows an $H-K$ versus $K-[12]$ diagram for the Galactic AGB stars. A clear separation between carbon- and oxygen-rich stars can be seen, with the carbon-rich stars showing significantly redder $H-K$ at the same $K-[12]$. The distinction holds up to $K-[12]=6$. The main reason for the difference between carbon-rich and oxygen-rich stars in this diagram is that in oxygen-rich Miras the silicate feature increases the 12-μm flux. The distinction is no longer clear once the circumstellar extinction becomes so large that the silicate band is no longer in emission. The stars with 9.8 μm in absorption fall below the carbon stars.

For the sources observed with TIMMI, we can compare the classifications obtained from this diagram with our measurements. This requires a small correction factor since the N band is not identical to the 12-μm band. We have calculated the correction factor for each of the LRS spectra in Fig. 8: we derive $N-[12]=0.3\pm0.1$ with no evidence for a colour term. This is only a minor correction to the plot.

Four sources (HV 12956, 04407 − 7000, 04498 − 6842 and 05112 − 6755) fall clearly on the oxygen-rich sequence. 05329 − 6709 falls on the extreme end of the relation where most Galactic stars are carbon stars but a few oxygen stars are also found; on the basis of this diagram the classification is inconclusive. Wood et al. (1992) detected OH emission from this source which suggests that the position of the object in the diagram is due to the silicate feature becoming self-absorbed. The classification derived from the diagram gives good agreement with those obtained from narrow-band photometry. We therefore suggest that the same relation as found for Galactic stars can be used for stars in the LMC.

The use of the relation is not so easy for the Magellanic Cloud sources not observed with TIMMI. The intrinsic uncertainties of the *IRAS* magnitudes, and to a lesser extent the variability, lead to estimated errors of ±1 mag in $K-[12]$. However, the diagram suggests that the objects with lower $H-K$ tend to be oxygen-rich. Ground-based mid-infrared photometry will be needed to apply this diagram to the faint LMC sources with more confidence. The success for the present sample indicates that for most of the sources only N-band photometry will be required.

05295 − 7121 falls below the relation, in a region avoided by Galactic AGB stars. For this object narrow-band photometry is not available, but the colours show it to be underluminous at 12 μm. The reason is not clear. It is possible that it has the silicate feature in absorption, or that it has considerable interstellar reddening rather than circumstellar. In either case, the object may be misclassified.

7.3 Lack of carbon stars?

Oxygen-rich AGB stars are known to extend to the highest bolometric magnitudes known for Magellanic Cloud AGB stars ($M_{bol} = -7.1$). In LMC globular clusters, carbon stars become predominant above a bolometric magnitude of -4.8 or $\log L_{\star} = 3.8$. Blanco et al. (1980) showed that this is also seen in the LMC bar. Lloyd Evans (1984) has shown that the transition from M to C occurs at higher luminosity in younger clusters. He also shows that the transition occurs abruptly, with very few weak-banded carbon stars. In the LMC the age and metallicity content of globular clusters are well correlated, and his results therefore indicate that younger, more metal-rich stars reach higher bolometric magnitudes as oxygen stars. The highly luminous, oxygen-rich AGB stars in our sample would then belong to such a young and relatively metal-rich population, with high-mass progenitors. Further observations will be required to see whether this applies to the full sample. It would be very interesting to find carbon stars among the obscured AGB stars in the LMC, and to investigate whether a lower-luminosity cut-off for such stars exists.

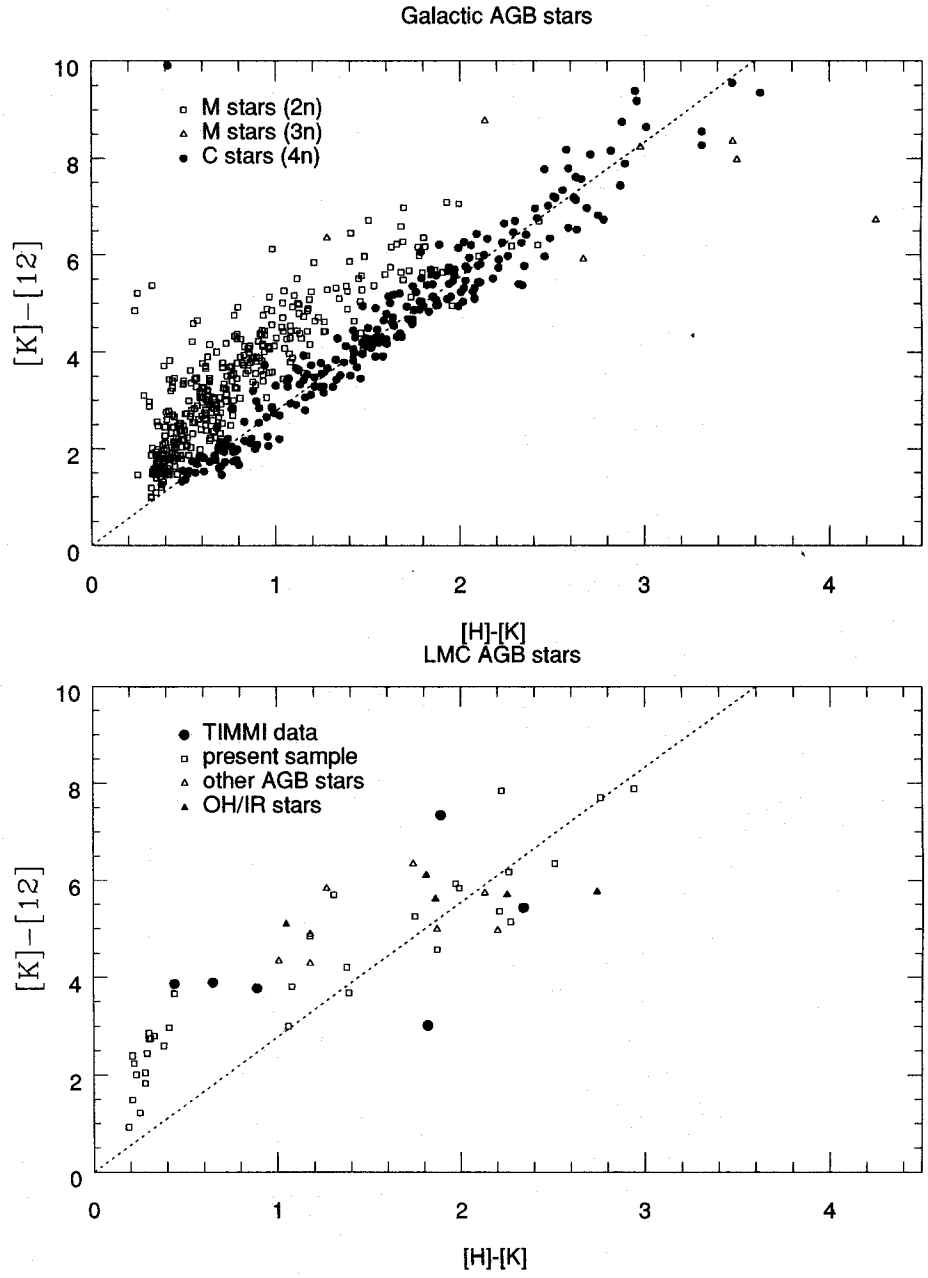

Figure 9. $K-[12]$ versus $H-K$. The upper diagram shows Galactic AGB stars and indicates two separate branches for oxygen-rich and carbon-rich stars. The lower diagram shows the data for the Magellanic Clouds stars. The filled circles indicate the sources observed with TIMMI.

It is noticeable that there is only one luminous ($\log L_\star = 4.3$) mass-losing carbon star known in the Magellanic Clouds (00554 – 7351: Wood et al. 1992 and Whitelock et al. 1989). It is possible that the near-infrared observations were not sensitive to mass-losing carbon stars, since carbon grains are more effective in absorbing stellar light than silicate (oxygen) grains. The detection limit at K of the survey was not much better than $K = 13$ mag, and there could be AGB stars in the Magellanic Clouds with significantly higher circumstellar extinction, about which we have no information as yet. Imaging observations at longer wavelengths are required to find such stars.

8 MASS-LOSS RATES

Many different methods have been used to estimate mass-loss rates for evolved stars. They all suffer from the problem that the observed species (e.g. CO, dust) constitutes only a minor fraction of the envelope and therefore requires a large correction factor which is not always well known. A good review of the available methods can be found in van der Veen & Olofsson (1989).

The best-understood method appears to involve using the CO emission (Knapp & Morris 1985; Mamon, Glassgold & Huggins 1988). This molecule is abundant and the emission is easily interpreted; it is therefore widely used for Galactic sources. However, CO emission from circumstellar envelopes is not observable at the distance of the LMC with present instruments. Jura (1986, 1987) has proposed to determine mass-loss rates for carbon stars using the observed *IRAS* 60-μm emission. The simplicity of this approach has led to its widespread use, even for oxygen-rich envelopes for which it was not derived originally. Even for Galactic sources, a reliable 60-μm flux is not always available, and for our LMC sources the Jura method cannot be directly applied.

There are a number of secondary methods available to estimate mass-loss rates. They are discussed in the following subsections. We will derive the *dust* mass-loss rates. For scaling to gas mass-loss rates a gas-to-dust ratio has to be assumed.

8.1 The 9.8-μm feature

Schutte & Tielens (1989) have presented detailed calculations of the strength of the 9.8-μm feature as a function of mass-loss rate and show that its strength and sign (emission or absorption) can be used as a determinant. They give a formula for the gas mass-loss rate as a function of the 10-μm optical depth, τ_{10}, which can be simplified if we assume that the velocities of the dust and the gas are equal and that the outflow velocity is constant. In terms of the dust mass-loss rate we obtain

$$M_{\rm dust} = 5 \times 10^{-4} 2\pi r_0 v_\infty \tau_{10} \qquad {\rm g\ s^{-1}}, \tag{3}$$

where r_0 is the inner radius of the shell, in cm, and v_∞ is the outflow velocity at infinity, in km s^{-1}. The constant arises from the absorption strength of the 10-μm feature. Taking $r_0 = 2 \times 10^{14}$ cm and $v_\infty = 10$ km s^{-1}, this becomes

$$M_{\rm dust} = 1 \times 10^{-8} \tau_{10} \qquad {\rm M_\odot\ yr^{-1}}. \tag{4}$$

However, converting the observed value of A_{10} to an optical depth is not easy, because of the competing effects of emission and self-absorption. The feature is strongest around $\tau_{10} \approx 0.2$ (Groenewegen, private communication) and goes into absorption around $\tau_{10} \approx 3.0$. Dust mass-loss rates for the sample observed with TIMMI would thus be less than 3×10^{-8} M$_\odot$ yr^{-1}. The curves in fig. 5 of Schutte & Tielens can also not be used for converting A_{10} to a mass-loss rate: the slope of the relation is very shallow and only two of the observed points fall near a model curve.

8.2 The near–mid-infrared colour temperature

A correlation between the $L - [12]$ colour (or related quantities) and the mass-loss rate derived with different methods has been noted by various authors (Nguyen-Q-Rieu et al. 1979; Jones, Hyland & Gatley 1983; Baud & Habing 1983; Schutte & Tielens 1989; Whitelock et al. 1994). The first two papers find it as a relation between the OH luminosity and the infrared colours.

Whitelock et al. (1994) calculate mass-loss rates by scaling the Jura formalism to the 25-μm *IRAS* flux density using scaling factors which differ for oxygen and carbon stars (see also Wood et al. 1992). For a large sample of Galactic AGB stars, they find a tight correlation between

Table 9. Dust mass-loss rates.

Name	mass-loss derived from: (K–[12])	(L–[12])	A_{10}	H–K	K–L	OH
00350–7436	–7.91	–7.25		–7.97	–8.17	
00483–7347	–7.69	–7.09		–7.77	–8.01	
00521–7054	–6.70	–6.51		–7.80	–7.59	
00554–7351	–6.92	–6.86		–7.28	–7.48	
HV12956	–7.48	–6.54	–7.73			
04286–6937	–6.74	–6.52		–7.51	–7.78	
04374–6831	–6.82	–6.74		–7.41	–7.52	
04407–7000	–7.86	–7.00	–7.95		–8.83	
04496–6958	–8.00	–7.48		–7.58	–7.88	
04498–6842	–6.64	–5.95	–6.31	–7.85	–8.11	
04509–6922	–7.79	–7.09		—	–8.12	
04516–6902	–7.61	–6.64		–8.07		
WOH SG061	–8.79					
04539–6821	–6.47	–6.79		–7.27	–7.40	
04545–7000	–6.77	–6.77		–7.02	–7.40	≤ –6.6
SP 30-6	–7.71					
04557–6753	–6.79	–7.47		–7.44	–7.49	
05003–6712	–7.33	–6.73		–7.89	–8.05	
05009–6616	–7.12	–6.45		–7.54	–7.59	
05099–6740	–6.68 (?)	–6.04(?)		–7.93	–8.53	
05112–6755	—	–6.17	–6.80	–7.27	–7.23	
05112–6739	—	–6.23		–7.52	–7.31	
LI-LMC0578	–7.51	–7.43		–7.85	–7.76	
05128–6455	–7.64	–7.26		–7.82	–7.91	
05190–6748	—	–6.79		–7.03	–7.21	
TRM088	–7.06	–7.01		–7.44	–7.66	
TRM045	–7.31			–7.51		
05291–6700	–8.33	–7.58		–8.27	–8.61	
05294–7104	–7.31	–6.52		–7.81	–8.51	
05295–7121	–7.16	–6.94		–7.55	–7.77	
05298–6957	–6.58	–6.74		–7.26	–7.19	≤ –6.1
05300–6651	–7.18	–7.24		–7.45	–7.63	
05316–6605	–7.92	–7.07			–8.77	
05329–6709	—	–5.75	–5.82	–6.81	–7.30	≤ –6.3
05348–7024	—			–6.63		
05360–6648	—			–7.23		
05402–6956	–6.87	–6.58		–7.29	–7.59	≤ –6.5
05506–7053	—	–6.16		–7.03	–7.11	
05558–7000	–7.55	–6.92		–7.90	–8.01	

these mass-loss rates and the $K-[12]$ colour. The relation breaks down at dust mass-loss rates above 5×10^{-8} $M_\odot$ yr^{-1} where the modification of the Jura equation is no longer valid. Since $K-[12]$ is well determined for our sample, we can apply this to our sources. The relation can be quantified as

$$\log(M_{\rm dust}) = 0.57(K-[12]) - 10.35, \quad (5)$$

where an expansion velocity of 10 km s^{-1} is used, which is more typical for Miras than the 15 km s^{-1} used by Jura (1987); the latter value may be more appropriate for high-mass-loss AGB stars. The equation applies for $K-[12]<5.5$.

Table 9 lists the resulting values for our sample of AGB stars. Dashes indicate that the colours fall far outside the range of applicability.

Schutte & Tielens (1989) derive a similar relation from their modelling described above, in terms of the infrared colour temperature, measured between 3.8 and 12.5 μm, and the mass-loss rate. Their relation extends to much higher mass-loss rates than the Whitelock et al. relation. From their fig. 5 we estimate the relation to be

$$\log(M_{\rm dust}) = 0.58(L'-[12]) - 8.97 \quad (6)$$

for dust mass-loss rates between 2×10^{-8} and 5×10^{-7} $M_\odot$ yr^{-1}. For higher values this approximation somewhat overestimates the result from Schutte & Tielens. Table 9 lists the derived values using the *IRAS* 12-μm flux. However, the Schutte & Tielens result uses the true dust continuum at 12 μm while the *IRAS* 12-μm flux includes a contribution from the silicate feature. This will lead to an overestimate of the mass-loss rate, which, judging from the $N-[9.8]$ colours of the TIMMI sample, may be as high as a factor of 4. We note that the calibration of Whitelock et al. uses the broad-band *IRAS* 12-μm magnitude. A separate column gives the result for the TIMMI sources using the [9.8] flux corrected for A_{10}. This correction significantly improves the agreement between the two methods.

8.3 The near-infrared optical depth

An alternative method for determining mass-loss rates is by using the optical depth of the envelope derived from near-infrared colours. This method was developed by Le Bertre (1987, 1988a,b; Epchtein, Le Bertre & Lépine, 1990), who modelled several variable carbon stars by solving the radiative transfer equation. The model uses a relation between the opacity at 1 μm and the colours $H-K$ and $K-L'$ (Epchtein et al., 1990, fig. 5). In the model it is assumed that: (1) the star emits like a blackbody with $T_\star=2200$ K; (2) the dust envelope is spherical; (3) the density law is $n(r)\propto r^{-2}$ and the expansion velocity is constant, corresponding to a constant mass-loss rate; (4) the inner radius of the dust shell, R_i, is such that the grain temperature at R_i is the condensation temperature for carbon grains, $T_c=900-1000$ K; (5) the dust emissivity law follows $Q(\lambda)\propto\lambda^\beta$. This is in principle valid only for carbon stars. The value of β that fits the energy distribution of carbon stars in the region 1–30 μm is $\beta=-1.0$ (e.g. Rouleau & Martin 1991). Le Bertre used $\beta=-1.3$ as suggested by Jura (1983). Assumptions (2), (3) and (5) are also used in the Jura formalism.

Table 10. Optical depth and near-infrared colours.

$\tau_{1\mu m}$	H–K	K–L′
.0	.84	0.91
.1	.88	1.01
.14	.89	1.05
.2	.91	1.10
.28	.94	1.16
.4	.98	1.25
.57	1.03	1.36
.8	1.10	1.49
1.13	1.20	1.66
1.6	1.33	1.86
2.26	1.51	2.10
3.2	1.75	2.40
4.53	2.05	2.84
6.4	2.46	3.32
9.05	3.05	3.96
12.8	3.85	4.80

The numerical relation between $\tau_{1\,\mu m}$ and $H-K$ and $K-L'$ is given in Table 10. We can now calculate the dust mass-loss rate using the following equations:

$$R_\star^2 = L_\star/(4\pi\sigma T_\star^4), \quad (7)$$

$$R_i^2\int Q_\lambda B_\lambda(T_c)\,{\rm d}\lambda = \frac{R_\star^2}{2}\int Q_\lambda B_\lambda(T_\star)\,{\rm d}\lambda, \quad (8)$$

$$M_{\rm d} = 16\pi a\rho\tau_{1\,\mu m}R_i V_e/3Q(1\ \mu{\rm m}), \quad (9)$$

with the following assumptions: $R_0\gg R_i$ (used in the third formula; R_0 is the outer radius of the dust shell); $T_c=950$ K; $Q(\lambda_{1\,\mu m})=0.19$; $a=0.1$ μm (grain size); $\rho=3$ g cm^{-3}, which is valid for carbon-rich dust (for silicates $\rho=2.7$); expansion velocity $V_e=10$ km s^{-1}. The derived values can be directly scaled to accommodate different values of $Q(1\ \mu m)$, the grain size, ρ, or the distance, without the need for numerical calculations.

Fig. 10 shows the fit of the Le Bertre track to our sample. It gives a fair fit, with a tendency for the sources to have a slightly too low $K-L$. Either this may be caused by molecular opacities distorting the spectrum, or the spread may indicate a range in stellar temperatures. We conclude that the colours are consistent with reddened blackbodies and that the Le Bertre formalism can in principle be applied.

We can approximate the above formulae as

$$M_{\rm d} = 7.53\times10^{11}\tau L_\star^{0.5} \quad (10)$$

in solar units. The resulting values are listed in Table 9. They are generally about 2.5 times lower than those derived with the previous method. The same effect is seen if we use the sample of Galactic Cap Miras of Whitelock et al. (1994), where the *HKL* colours would indicate $\tau=0$. A possible explanation is that the central-star temperatures are higher than assumed here, of the order of 3000 K rather than 2200 K. There are several other uncertainties inherent in

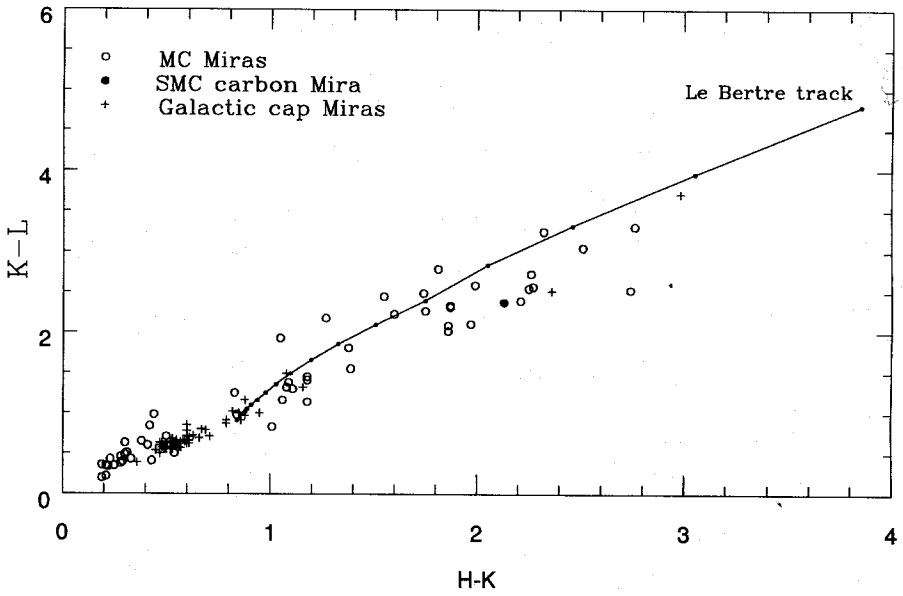

Figure 10. $K-L$ versus $H-K$ for the Magellanic Clouds Stars. For comparison the Galactic Cap Miras from Whitelock et al. (1994) are also shown. The line indicates the reddening track calculated by Le Bertre.

the above simplifications. The most important may be that equation (10) is derived for carbon stars, whereas the majority of the stars in our sample may be oxygen-rich. However, the Le Bertre track could give a good approximation of the *relative* mass-loss rates of the stars in our sample. We could in fact re-calibrate it using the Whitelock relation, which would imply adding approximately 0.4 to $\log \dot{M}$ derived from the Le Bertre method.

We note that this relation implies that the observational $H-K$ versus $K-[12]$ relation discussed in the previous section in fact traces the mass loss.

8.4 OH luminosity

Baud & Habing (1983) have shown that there is a correlation between OH maser strength and mass-loss rate. This is in fact to be expected if the masers are saturated and operate at maximum pumping efficiency. The maser is pumped by a transition at a wavelength of 35 μm, and the theoretical efficiency for converting 35-μm photons to OH maser photons is 25 per cent. In this case the maser 'measures' the infrared continuum at 35 μm and the Jura formula applies with a wavelength shift from 60 μm to 35 μm. It is noteworthy that the maser strength is determined by the infrared flux and not by the number of OH molecules. Thus, the OH luminosity is dependent on the *dust* mass-loss rate and not the OH gas mass-loss rate! This method was used by Wood et al. (1992) to derive mass-loss rates for their OH-emitting stars in the LMC.

The calibration by Baud & Habing was performed with a small sample and has not been refined. Many more Galactic Miras with OH emission are now known, and a re-investigation of the method is possible. This is especially important because the newly discovered OH-emitting stars in general show pump efficiencies below the theoretical value of 25 per cent.

A catalogue of OH-emitting stars can be found in te Lintel Hekkert et al. (1991). We have cross-correlated this catalogue with the Galactic CO catalogue of Loup et al. (1993) which also gives mass-loss rates derived from the CO emission. The distance is calculated by assuming a bolometric luminosity of 10^4 $L_\odot$.

Figs 11(a)–(c) show a comparison of the different methods used to calculate mass-loss rates for these Galactic stars. The filled circles indicate sources for which $L_{OH} > 200$ Jy kpc^2 which is the OH luminosity of the faintest detected sources in the LMC. (The five stars are $26.5+0.6$, $30.1-0.7$, $32.8-0.3$, $104.9+2.4$ and $127.9-0.0$; $32.8-0.3$ has no 60-μm detection.) The correlation with the CO mass-loss rates is poor. For the brightest OH emitters, the CO implies mass-loss rates that are much too low. This has been noted before (Heske et al. 1990). Van der Veen & Rugers (1989) suggest that this occurs when the CO excitation line at 4.6 μm becomes optically thick, but this may not be the correct explanation since collisional excitation is dominant over radiative excitation. Alternatively, Schutte & Tielens (1989) discuss the possibility that the mass-loss rate was lower in the past, and that the CO emission is still dominated by material far from the the star dating back to earlier times. Recently, Groenewegen (1994) has found evidence for this in the case of OH32.8 – 0.4. In either case the Jura method would give better values for the present-day mass-loss rate than would the CO emission.

The OH mass-loss rates, calculated as in Baud & Habing, show a general correlation with the Jura values, although there is significant disagreement at the higher values. The scatter is in part due to the range in pump efficiency: calculating the ratios of the 25-μm *IRAS* flux of this sample and the OH peak flux densities shows efficiencies in the range of 1–20 per cent, with large scatter. However, the disagree-

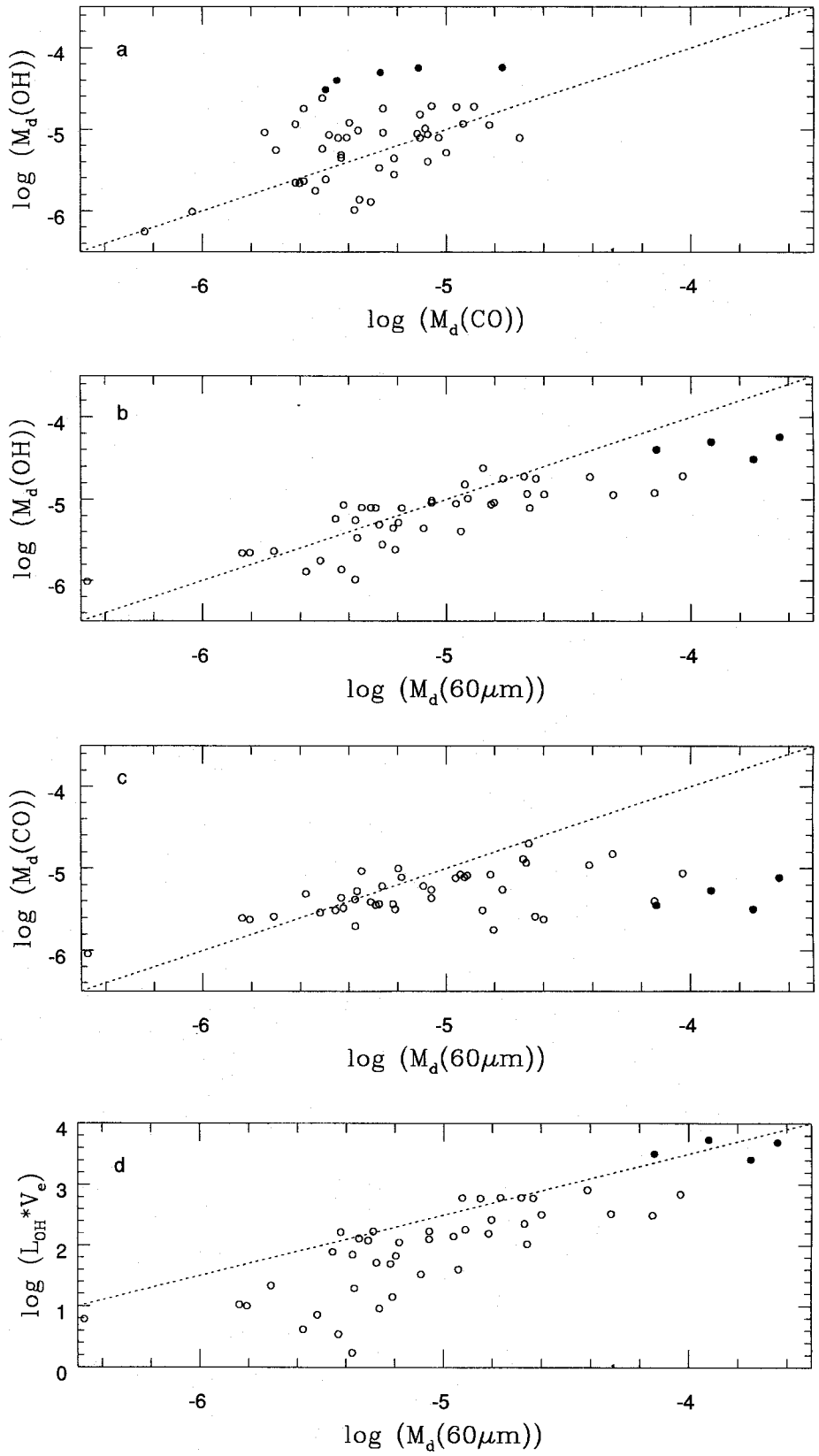

Figure 11. Comparison between dust mass-loss rates derived from CO, 60-μm flux and OH luminosity, for a sample of Galactic OH/IR stars. The filled circles indicate Galactic stars with $L_{OH} > 200$ Jy kpc^{-2} which would have been detectable at the distance of the LMC. The 60-μm emission is assumed to give the most reliable value. The OH mass-loss rate is calculated as in Baud & Habing (1983). Panel (d) shows a relation between L_{OH} and the 60-μm mass-loss rate. The line gives our proposed calibration for OH masers which operate at maximum pumping efficiency.

ment at the high mass-loss rates indicates a need for a closer look at the method.

Baud & Habing assume that the surface brightness of the OH maser is approximately constant and therefore that $L_{OH} \sim (M_d/V_e)^2$. This assumption will be incorrect if the OH strength is dependent on the dust radiation, in which case $L_{OH} \sim M_d/V_e$ (calculating L_{OH} as described in Baud & Habing). Fig. 11(d) shows the observed data. Drawing a line through the higher points only, to eliminate the sources with low OH pump efficiencies, we obtain approximately

$$\log M_{dust} = \log (L_{OH} V_{exp}) - 9.8. \quad (11)$$

The uncertainties are large, because few OH emitters operate at peak efficiency. Equation (11) will therefore, for most stars, give lower limits to the mass-loss rates. In addition, the measurement uncertainties in the OH peak flux densities are large for the Magellanic Cloud objects. The derived values are listed in Table 9. There is reasonable agreement with the $K-[12]$ and $L-[12]$ methods.

8.5 The 12-μm/25-μm flux ratio

Van der Veen & Olofsson (1989) also discuss mass-loss rates derived from the ratio of the *IRAS* 12-μm and 25-μm fluxes. This is an attractive method which depends only on the dust temperature which in turn is determined by the optical depth of the shell and chemical composition. However, the calculated mass-loss rates correlate poorly with values determined by other methods, most noticeably CO (Whitelock et al. 1994; Epchtein et al. 1990). There is a general trend of redder *IRAS* colours with higher mass-loss rates, but with large scatter. It is possible that the derived values are sensitive to long-term fluctuations in the mass-loss rate; Whitelock et al., on the other hand, conclude that the optical depth through the shell is not the dominant factor controlling the 25-μm to 12-μm flux ratio.

For our sample this is aggravated by the fact that the 25-μm flux is the least reliable of the available data points. We have therefore chosen not to apply this method. Better mid-infrared data (e.g. from *ISO*) are needed to investigate the applicability of the method.

8.6 Results

The values for the mass-loss rates determined from the ratio of near-infrared to mid-infrared emission are preferred, since these methods are quite well calibrated. The $L-[12]$ values should still be corrected for silicate emission and presently are overestimated. The near-infrared colour method probably gives reasonable *relative* mass-loss rates but the absolute calibration is uncertain; the present results indicate that this method underestimates the mass-loss rate by a factor of 2.5 on average. For one object (05099 – 6740) there is doubt whether the *IRAS* source is associated with the star and the mass-loss rates are marked accordingly.

We have not discussed the problem of source variability. For the methods using colours, in principle simultaneous measurements are required: this is a potential problem wherever *IRAS* data are used. The results of Whitelock et al. (1994), who find good agreement for the $K-[12]$ mass-loss rates with values derived from CO, suggest that in many cases the effect of variability on the *IRAS* fluxes is small. However, the effect may well be larger for the present sample, which contains more luminous stars. The *IRAS* data are likely biased towards the peak of the pulsation cycle whereas the near-infrared data are taken at a random phase: the near-infrared–mid-infrared methods may therefore overestimate the mass-loss rates by a factor of 2–5. More accurate mass-loss rates will require monitoring over a full period at a range of wavelengths.

There appears to be no simple way to determine gas mass-loss rates directly for Magellanic Cloud stars. We can derive only dust mass-loss rates which have to be scaled by an uncertain factor. We find a large range of dust mass-loss rates. If we assume a gas-to-dust ratio of 400, the resulting gas mass-loss rates would be between 5×10^{-4} and 4×10^{-6} $M_\odot\ yr^{-1}$. The highest value is found for 05329 – 6709 which is also one of the brightest *IRAS* sources in the sample and has a very high bolometric luminosity. However, for the full sample there is no evidence of a correlation between mass-loss rates and luminosity. We also find no evidence that the mass-loss rates in the SMC are systematically lower than in the LMC. This result would not be unexpected if the highest values of $\dot{M}$ were limited by the momentum in the radiation field, as suggested by Vassiliadis & Wood (1993).

9 EXPANSION VELOCITIES

Expansion velocities are available for only four of the *IRAS*-detected AGB stars in the LMC, all based on the OH detections by Wood et al. (1992). These four objects can be compared to Galactic AGB stars. Wood et al. find that the OH expansion velocities of LMC AGB stars are 40 per cent lower than those of Galactic OH/IR stars of similar *IRAS* colours. This difference is particularly clear when expansion velocity is plotted against period. For this comparison, Wood et al. use only Galactic stars within 1° of the Galactic plane, selecting highly luminous sources.

We can apply the same procedure to the sample of Galactic OH/IR stars used in Section 8.4. The comparison is shown in Fig. 12. Note that we plot expansion velocity rather than the ΔV used by Wood et al. Our Galactic sample contains five objects with OH luminosities similar to those of the MC stars, although this depends on distances which are uncertain. The upper panel shows that, compared with the Galactic star velocities, the LMC expansion velocities may indeed be lower, but not by as large a factor as found by Wood et al. The difference in conclusion is mostly caused by the fact that we use half the total width of the profile rather than half the separation of the two highest maser peaks to define the expansion velocity. The difference can be several km s^{-1} in the case of noisy profiles.

The middle panel of Fig. 12 shows the comparison as a function of the *IRAS* colour. The five luminous Galactic stars are indicated by crosses. They show *IRAS* colours that are comparable to those of the LMC stars. The lower panel gives the expansion velocity versus period, the latter from van Langevelde, van der Heiden & van Schooneveld (1990). The LMC sources appear very similar to the luminous Galactic OH/IR stars. Their expansion velocities appear to be lower by about 10–20 per cent although there are insuffi-

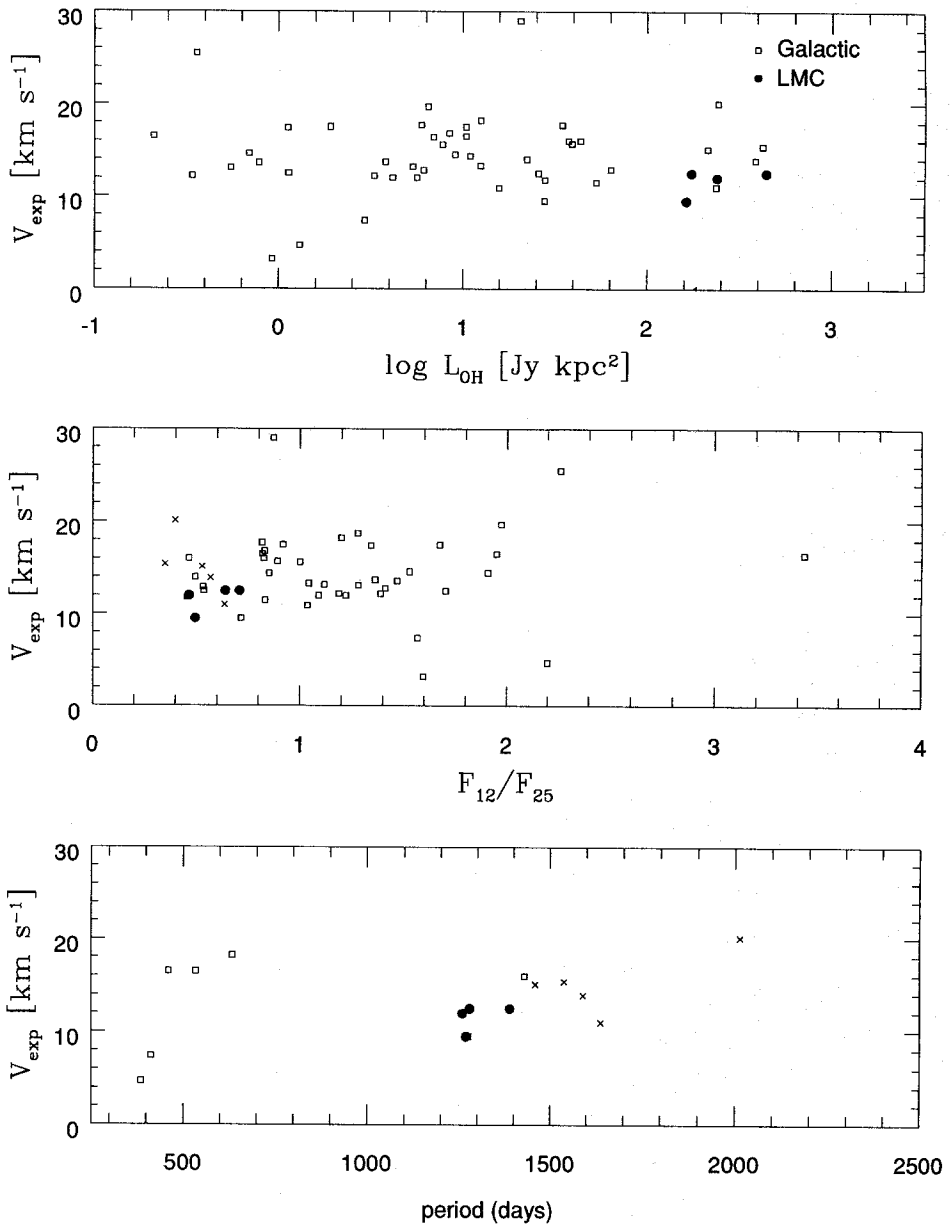

Figure 12. Expansion velocities of LMC and Galactic OH/IR stars. The crosses indicate Galactic OH/IR stars of comparable OH luminosity to the LMC sources.

cient data to draw a firm conclusion. Higher sensitivity OH observations would be desirable to define better the expansion velocities of the LMC stars.

Almost all other MC sources in our sample have F_{12}/F_{25} close to unity, which is significantly bluer than the OH-detected sources. Compared with the Galactic sources in the middle panel, we expect that their OH emission will be considerably fainter than the detection limit of the Parkes observations (Wood et al. 1992).

10 PERIOD DETERMINATION

Two of the sources in our sample have been monitored at SAAO in the past: HV 12956 (Whitelock et al. 1989) and 04407 – 7000 (unpublished). 04407 – 7000 was discovered and monitored as part of a programme on AGB stars in the Galactic cap; it was later dropped because of its probable association with the LMC. 05329 – 6709 was monitored by Wood et al. (1992), who derive a period of 1260 d. In addition, Wood et al. give periods for a number of other *IRAS* stars in the Magellanic Clouds.

HV 12956 is a known optical variable, for which a period of 517 d has been derived (Payne-Gaposchkin & Gaposchkin 1966). Its spectral type is M5e at maximum which is late for an SMC object (Whitelock et al. 1989). The present observations confirm the association of the *IRAS* source with the Harvard variable: Whitelock et al. considered this as less certain because the colours of the star are not obviously reddened.

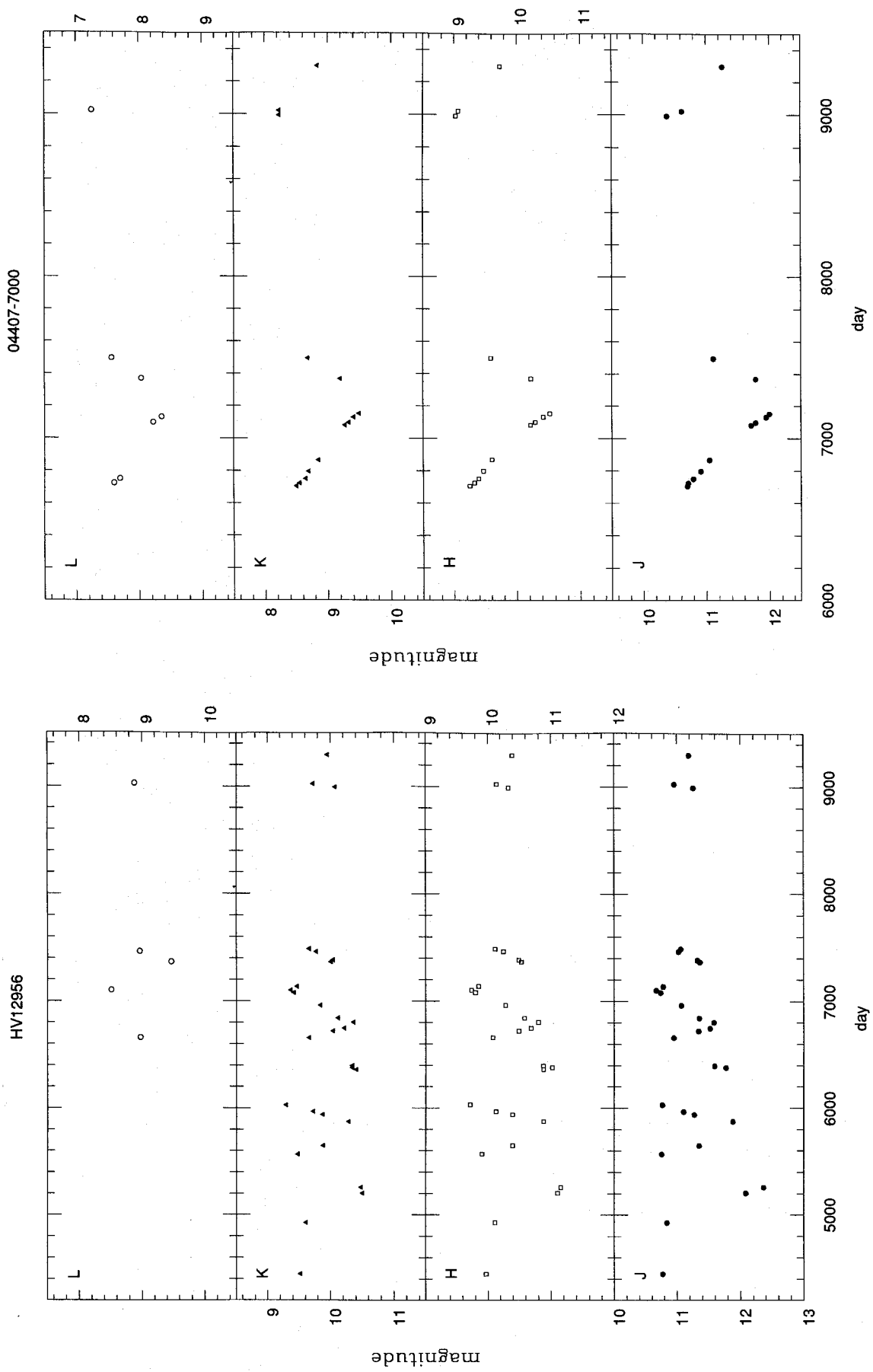

Figure 13. Monitoring data for HV 12956 and 04407 − 7000. The latter requires more data to allow an unambiguous period determination.

Fig. 13 shows the variation of the infrared magnitudes including both the previous and the new observations. The most recent SAAO observations of 1993 November and the IRAC photometry are also included. For HV 12956 there are sufficient data for an unambiguous determination of the period. Using a program written by Luis Balona, we obtain 515 d, with a nominal uncertainty of 2 d. A period can also be derived by comparing the Julian Date at maximum given by Payne-Gaposchkin & Gaposchkin, JD 243 1436, with the best-determined infrared maximum at JD 244 7100. This gives a period of 522 ± 1 d which should be regarded as an upper limit because the infrared maximum typically lags 0.1 to 0.2 of a cycle behind the optical maximum (Lockwood & Wing 1971; Strecker 1973). For 04407 – 7000 there are two possible periods: 1220 d or 770 d. Further monitoring is needed before either of these can be excluded. Both sources have long periods compared with optical Miras (e.g. Whitelock et al. 1991) and are similar to the Wood et al. sources. They also have bright bolometric magnitudes ($M_{bol} = -7.2$ for 04407 – 7000 and $M_{bol} = -6.7$ for HV 12956), consistent with the suggestion that long periods are reached only for stars with high-mass progenitors.

For HV 12956 a longer modulation is also clear from Fig. 14. Neither the time-scale for this modulation nor its regularity can be determined from the available data. Such modulations are commonly seen in long-period Miras. It is possible that similar, but smaller-amplitude, changes occur in shorter-period Mira where they are less obvious.

Optical Miras show a strong period–luminosity relation, with higher luminosity coinciding with longer periods. The relation is quite narrow in the K band; it shows more scatter when the bolometric luminosity is used. A discussion of the period–luminosity diagram for LMC Miras is given by Feast et al. (1989), based on stars with periods less than 420 d. Fig. 14 shows their data together with the present sample. Clearly the long-period sources are more luminous than would be predicted by extrapolating from the optical variables. This is consistent with other long-period variables in the LMC (Feast et al. 1989; Wood et al. 1983; Wood et al. 1992; see fig. 20 in Vassiliadis & Wood 1993). The period–luminosity relation used by Wood (1989) and Vassiliadis & Wood is aimed at fitting these longer-period stars and therefore is significantly steeper than commonly used period–luminosity relations: it does not fit the shorter-period variables well (Groenewegen 1995). Feast et al. (1989) show that a period–luminosity–colour relation using the $J-K$ colour fits the short-period variables better. This cannot be directly used for the long-period variable stars where the $J-K$ colour is affected by circumstellar extinction.

The fit to the carbon-rich stars in Fig. 14 is clearly different from that to the oxygen-rich stars. Glass et al. (1987) have suggested that the high molecular opacities of carbon atmospheres in the J and H bands cause the bolometric luminosity to be underestimated. In addition, interband water-vapour absorption in oxygen Miras may cause their luminosity to be slightly overestimated. This effect should be understood before carbon and oxygen Miras can be compared. We note that the 'peculiar' source HV 12956 falls about 2 mag above the relation. If it were indeed a foreground object, it would still have to be at a distance of around 20 kpc and 10 kpc above the Galactic plane. An association with the SMC itself seems more likely.

The period–luminosity relation has been interpreted as an evolutionary sequence, but this is unlikely for several reasons: (1) the Mira lifetimes ($\sim 10^5$ yr) are too short to give an appreciable evolution in luminosity; (2) Miras in individual globular clusters show a very small range in luminosity; and (3) for Galactic Miras the velocity dispersion is a function of period (Feast 1963). An alternative suggestion is that the long-period variables with periods larger than 1000 d originate from a change from overtone to fundamental pulsation mode. However, this would result in a horizontal translation in Fig. 14, while we observe that the stars with the longest periods are shifted upward with respect to shorter-period stars. Thus, the likely explanation for the long-period Magellanic Cloud stars is that they originate from higher-mass progenitor stars (e.g. Feast et al. 1989) (see also the discussion in Whitelock et al. 1991). The fact that long periods as shown by the Magellanic Cloud Miras are not found in the outer bulge (Whitelock et al. 1991), where a population with massive progenitors is not present, also favours the theory that long periods arise from a young, relatively high-mass stellar population.

The evolutionary models of Vassiliadis & Wood (1993) explain the observed distribution of periods with luminosity quite well: here the spread at any given luminosity is largely caused by the fact that the mass of the star decreases because of mass loss, increasing its period. This effect is largest for massive stars and could be the cause of the absence of a clearly defined period–luminosity relation for AGB stars with long periods. The evolutionary tracks of Vassiliadis & Wood (1993) in the period–luminosity diagram are inclined to the observed period–luminosity relation, following a much shallower angle. This is in very good agreement with a period–luminosity relation found for globular clusters, connecting semi-regular variables with the Miras (Whitelock 1986). The only difference is that the observed globular cluster relation is shifted to shorter periods with respect to the theoretical predictions (Zijlstra 1995). It seems likely that this shallow relation is the true evolutionary sequence, and that the observed period–luminosity relation of Fig. 14 mainly traces a range of initial masses.

11 CONCLUSIONS

We have presented the results of an infrared survey of *IRAS* sources in the Magellanic Clouds. We find a significant number of obscured AGB stars, constituting an additional AGB population to the low-mass-loss, short-period Miras already known. We present positions and near-infrared photometry. The stars are highly luminous, with luminosities in general between $\log L = 4.0$ and $\log L = 4.7$. 10-μm photometry in several bands has been performed for a number of these sources; the results indicate that oxygen-rich shells dominate. Two of the sources show a very strong silicate feature, which in our Galaxy is found only for low-luminosity *IRAS* sources. It is shown that oxygen and carbon stars can be separated on the basis of near-infrared–mid-infrared colours: the relation is valid for both Galactic and Magellanic Cloud stars. However, the uncertainties in the *IRAS* data are too large to allow one to use this relation in

the Magellanic Clouds directly; instead, ground-based 10-μm data should be used.

We discuss several methods to obtain mass-loss rates. The gas mass-loss rate cannot be directly determined for these sources and we have only been able to derive dust mass-loss rates. The $K-[12]$ and $L-[12]$ colours give the preferred estimates of the mass-loss rates, since these methods are well calibrated against CO mass-loss rates and correlate well with those. In principle the near-infrared colours allow one to measure the optical depth through the shell, although the models yield only relative mass-loss rates. We give a new relation to derive approximate mass-loss rates from the OH luminosity.

The LMC sources appear to show slightly lower expansion velocities than Galactic OH/IR stars, although the difference may not be as large as found by Wood et al. (1992). Overall the obscured AGB stars in the Magellanic Clouds are quite similar to the (relatively few) luminous Galactic OH/IR stars.

For two of the sources we are able to derive periods. For

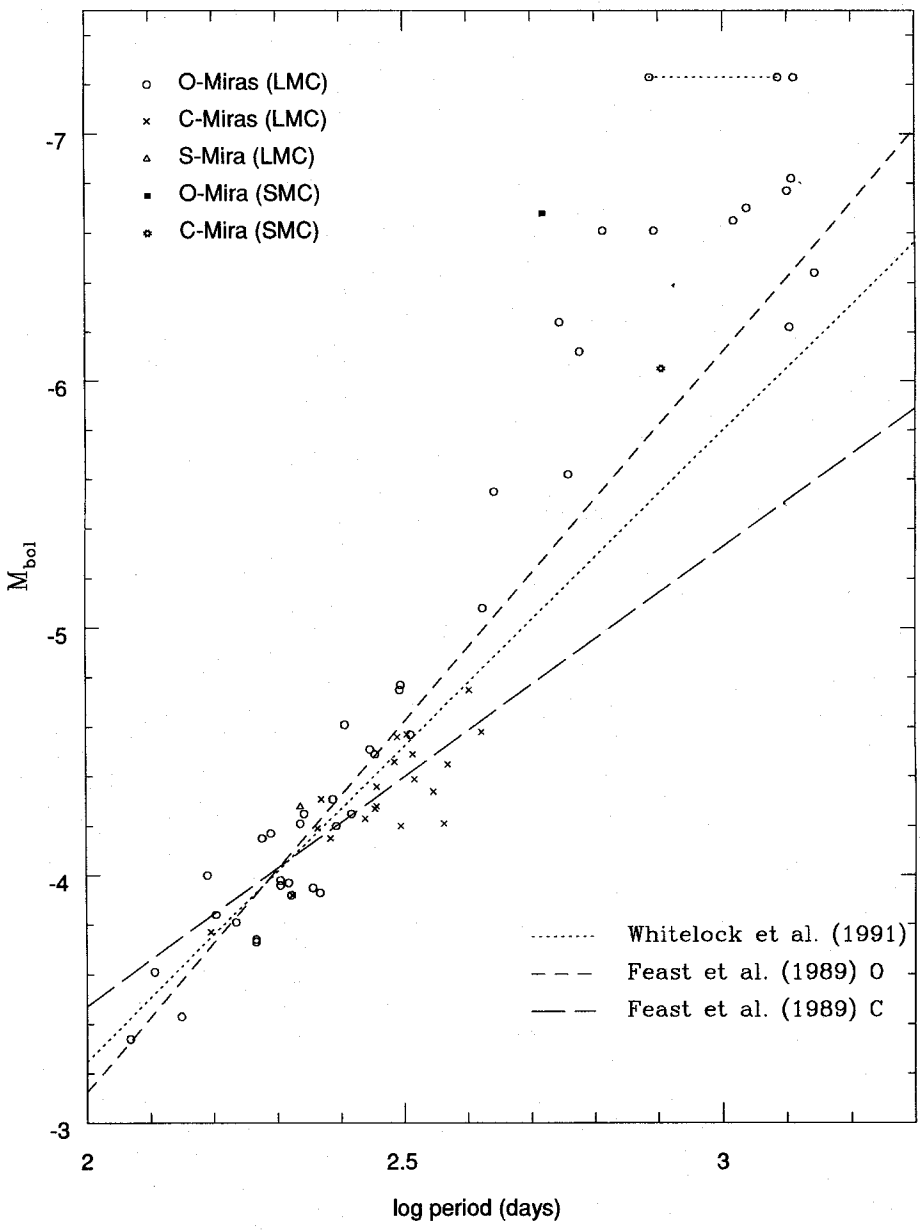

Figure 14. Period–luminosity relation for Magellanic Cloud Miras. The horizontal line indicates two possible periods for a single object. The dashed lines show the relations proposed by Feast et al. (1989) for oxygen and carbon Miras; the dotted line shows the calibration for Galactic sources of Whitelock et al. (1991).

several other objects, periods were already known. All periods are very long ($P \gtrsim 1000$ d), with one exception (the SMC source HV 12956), and all stars fall above the period–luminosity relation as derived for short-period Miras. It is likely that the short-period and long-period AGB stars have different progenitor stars and are not evolutionarily related, where long periods are derived from high-mass progenitors. The sensitivity limit of *IRAS* is insufficient to detect the circumstellar envelopes of low-luminosity AGB stars. *ISO* observations will be needed to study the mass loss of these stars. An analysis of how the mass loss depends on the characteristics of the progenitor stars will require such *ISO* observations.

ACKNOWLEDGMENTS

This paper is based on observations obtained at the European Southern Observatory and the South African Astronomical Observatory. We have made use of the infrared archive at the SAAO for this research and of the SIMBAD data base. We thank Robin Catchpole and Michael Feast for the earlier observations of HV 12956 and 04407 – 7000 used in this paper. We would also like to thank the supporting staff at ESO and SAAO, in particular Andrea Monetti, Hans-Ulrich Käufl and Francois van Wijk, for their help during the observations. We thank Xander Tielens for sending us the data used in Schutte & Tielens (1989), and Bruno Leiblundgut for the critical reading of the manuscript.

REFERENCES

Baud B., Habing H. J., 1983, A&A, 127, 73
Bessell M. S., Brett J. M., Scholz M., Wood P. R., 1989a, A&A, 213, 209
Bessell M. S., Brett J. M., Scholz M., Wood P. R., 1989b, A&AS, 77, 1
Blanco V. M., McCarthy M. F., Blanco B. M., 1980, ApJ, 242 938
Blöcker T., Schönberner D., 1991, A&A, 244, L43
Bouchet P., Moneti A., Slezak E., Le Bertre T., Manfroid J., 1989, A&AS, 80, 379
Carter B. S., 1990, MNRAS, 242, 1
Chiosi C., Maeder A., 1986, ARA&A, 24, 329
Elias J. H., Frogel J. A., Schwering P. B. W., 1986, ApJ, 302, 675
Epchtein N., Le Bertre T., Lépine J. R. D., 1990, A&A, 227, 82
Feast M. W., 1963, MNRAS, 125, 367
Feast M. W., Walker A. R., 1987, ARA&A, 25, 345
Feast M. W., Robertson B. S. C., Catchpole R. M., Lloyd Evans T., Glass I. S., Carter B. S., 1982, MNRAS, 201, 439
Feast M. W., Glass I. S., Whitelock P. A., Catchpole R. M., 1989, MNRAS, 241, 375
Feast M. W., Whitelock P. A., Carter B. S., 1990, MNRAS, 247, 227
Fouqué P., Le Bertre T., Epchtein N., Guglielmo F., Kerschbaum F., 1992, A&AS, 93, 151
Glass I. S., Catchpole R. M., Feast M. W., Whitelock P. A., Reid I. N., 1987, in Kwok S., Pottasch S. R., eds, Late Stages of Stellar Evolution. Reidel, Dordrecht, p. 51
Groenewegen M. A. T., 1994, A&A, 290, 544
Groenewegen M. A. T., 1995, in Watt G. D., Williams P. M., eds, Proc. Conf. Circumstellar Matter, Edinburgh, Astrophysics and Space Science. Kluwer, Dordrecht, p. 321
Guglielmo F., Epchtein N., Le Bertre T., Fouqué P., Hron J., Kerschbaum F., Lépine J. R. D., 1993, A&AS, 99, 31
Han Z., Podsialowski Ph., Eggleton P. P., 1994, MNRAS, 270, 121
Hearn A. G., 1989, in Mennessier M. O., Omont A., eds, From Miras to Planetary Nebulae: Which Path for Stellar Evolution? Editions Frontières, Gif-sur-Yvette, p. 121
Heske A., Forveille T., Omont, A., van de Veen W. E. C. J., Habing H. J., 1990, A&A, 239, 173
Hughes S. M. G., Wood P. R., 1990, AJ, 99, 784
Jones T. J., Hyland A. R., Gatley I., 1983, ApJ, 273, 660
Jura M., 1983, ApJ, 267, 647
Jura M., 1986, ApJ, 303, 327
Jura M., 1987, ApJ, 313, 743
Käufl U., Jouan R., Lagage P. O., Masse P., Mestreau P., Tarrius A., 1992, The Messenger, 70, 67
Knapp G. R., Morris M., 1985, ApJ, 292, 640
Le Bertre T., 1987, A&A, 176, 107
Le Bertre T., 1988a, A&A, 190, 79
Le Bertre T., 1988b, A&A, 203, 85
Le Bertre T., 1993, A&AS, 997, 729
Lloyd Evans T., 1984, MNRAS, 208, 447
Lockwood G. W., Wing R. F., 1971, ApJ, 169, 63
Loup C., Forveille T., Omont A., Paul J. F., 1993, A&AS, 99, 291
Loup C., Zijlstra A. A., Waters L. B. F. M., 1995, A&AS, in press (Paper I)
McGregor P. M., 1994, PASP, 106, 508
Mamon G. A., Glassgold A. E., Huggins P. J., 1988, ApJ, 328, 797
Nguyen-Q-Rieu, Laury-Micoulaut C., Winnberg A., Schultz G. V., 1979, A&A, 75, 351
Payne-Gaposchkin C., Gaposchkin S., 1966, Smithson. Contrib. Astrophys., 9, 1
Pottasch S. R., Bignell C., Olling R., Zijlstra A. A., 1988, A&A, 205, 248
Rebeirot E., Martin N., Mianes P., Prévot L., Robin A., Rousseau J., Peyrin Y., 1983, A&AS, 51, 277
Reid I. N., 1991, ApJ, 382, 143
Reid I. N., Tinney C. G., Mould J. R., 1990, ApJ, 348, 98
Robertson B. S. C., Feast M. W., 1981, MNRAS, 196, 111
Rouleau F., Martin P. G., 1991, ApJ, 377, 526
Sandulaek N., 1970, Contrib. Cerro-Tololo Obs., 89
Sandulaek N., Philip A. G., 1977, Publ. Warner and Swasey Obs., 2, No. 5
Schutte W. A., Tielens A. G. G. M., 1989, ApJ, 343, 369
Schwering P. B. W., 1989, A&AS, 79, 105
Schwering P. B. W., Israel F. P., 1989, A&AS, 79, 79
Schwering P. B. W., Israel F. P., 1990, A catalog of IRAS sources in the Magellanic Clouds. Kluwer, Dordrecht
Shore S. N., Sandulaek N., 1984, ApJS, 55, 1
Smith V. V., Lambert D. L., 1989, ApJ, 345, L75
Smith V. V., Lambert D. L., 1990, ApJ, 361, L69
Smith V. V., Plez B., Lambert D. L., Lubowich D. A., 1994, ApJ, 441, 735
Strecker D. W., 1973, Univ. Minnesota Astrophys. Rep. No. 15
te Lintel Hekkert P., Caswell J. L., Habing H. J., Haynes R. F., Norris R. P., 1991, A&AS, 90, 327
Tinney C. G., Mould J. R., Reid I. N., 1993, AJ, 105, 1045
van der Veen W. E. C. J., Olofsson H., 1989, in Mennessier M. O., Omont A., eds, From Miras to Planetary Nebulae: Which Path for Stellar Evolution? Editions Frontières, Gif-sur-Yvette, p. 139
van der Veen W. E. C. J., Rugers M., 1989, A&A, 226, 183
van Langevelde H. J., van der Heiden R., van Schooneveld C., 1990, A&A, 239, 193
Vassiliadis E., Wood P. R., 1993, ApJ, 413, 641
Weideman V., 1987, A&A, 188, 74
Westerlund B. E., Olander N., Hedin B., 1981, A&AS, 43, 267
Whitelock P. A., 1986, MNRAS, 219, 525

Whitelock P. A., Feast M. W., Menzies J. W., Catchpole R. M., 1989, MNRAS, 238, 769
Whitelock P. A., Feast M. W., Catchpole R. M., 1991, MNRAS, 248, 276
Whitelock P. A., Menzies J. W., Feast M. W., Marang F., Carter B. S., Roberts G., Catchpole R. M., Chapman J. W., 1994, MNRAS, 267, 711
Wood P. R., 1989, in Mennessier M. O., Omont A., eds, From Miras to Planetary Nebulae: Which Path for Stellar Evolution?. Editions Frontières, Gif-sur-Yvette, p. 21
Wood P. R., Bessell M. S., 1985, PASP, 97, 681
Wood P. R., Bessell M. S., Fox M. W., 1983, ApJ, 272, 99
Wood P. R., Whiteoak J. B., Hughes M. G., Bessell M. S., Gardner F. F., Hyland A. R., 1992, ApJ, 397, 552
Zijlstra A. A., 1995, in Watt G. D., Williams P. M., eds, Proc. Conf. Circumstellar Matter, Edinburgh, Astrophysics and Space Science. Kluwer, Dordrecht, p. 309
Zijlstra A. A., van Hoof P. A. M., Chapman J. M., Loup C., 1994, A&A, 290, 228